JOINT CAPACITY OPTIMIZATION OF RENEWABLE GENERATION AND HYBRID ENERGY STORAGE FOR MICRO-GRIDS

BY

UMER AKRAM

A Thesis Presented to the
DEANSHIP OF GRADUATE STUDIES

KING FAHD UNIVERSITY OF PETROLEUM & MINERALS

DHAHRAN, SAUDI ARABIA

In Partial Fulfillment of the
Requirements for the Degree of

MASTER OF SCIENCE

In

ELECTRICAL ENGINEERING

November 2017

KING FAHD UNIVERSITY OF PETROLEUM & MINERALS
DHAHRAN 31261, SAUDI ARABIA

DEANSHIP OF GRADUATE STUDIES

This thesis, written by UMER AKRAM under the direction of his thesis adviser and approved by his thesis committee, has been presented to and accepted by the Dean of Graduate Studies, in partial fulfillment of the requirements for the degree of MASTER OF SCIENCE IN ELECTRICAL ENGINEERING.

Thesis Committee

Dr. Muhammad Khalid (Adviser)

Dr. Muhmoud Kassas (Member)

Dr. Salim Ibrir (Member)

Dr. Ali Ahmad Al-Shaikhi
Department Chairman

Dr. Salam A. Zummo
Dean of Graduate Studies

23/11/17
Date

I dedicate this thesis to my whole family, especially my parents and brother Umair Akram, whose love, affection, guidance, and unselfish support have laid the foundations of this accomplishment.

ACKNOWLEDGMENTS

All the praise is due to Allah and peace be upon the Prophet Muhammad and his family, his companions (may Allah be please with them), and his followers.

With the immense respect, I would like to extend my deepest gratitude to Dr. Muhammad Khalid for his guidance and support. It has been my honor to be able to work with him. His constant motivation helped me to produce quality work. I would like to thank my committee members: Dr. Mahmoud Kassas and Dr. Salim Ibrir for their useful response, advice, and time they spent reviewing this thesis. I am very obliged to Electrical Engineering Department at King Fahd University of Petroleum & Minerals (KFUPM) for providing the excellent research environment. I also acknowledge the support provided by the Deanship of Research (DSR) at King Fahd University of Petroleum & Minerals (KFUPM) for funding this work. Also, I would like to thank Research Institute (RI) at KFUPM and Saudi Electricity Company (SEC) for providing renewables and demand data to carry out this research. In particular, I appreciate the support of Mr. Hussain A. Al-Harthi for arranging time series data.

TABLE OF CONTENTS

LIST OF TABLES

LIST OF FIGURES

LIST OF ABBREVIATIONS

BES	Battery Energy Storage
BESS	Battery Energy Storage System
BSA	Battery Sizing Algorithm
DG	Diesel Generator
ERBC	Emissions Reduction Benefit Cost
ESS	Energy Storage System
EV	Electric Vehicle
FC	Fuel Cell
GA	Genetic Algorithm
GHG	Greenhouse Gases
HESS	Hybrid Energy Storage System
HH	Hub Height
HPGS	Hybrid Power Generation System
MG	Microgrid

PCC	Point of Common Coupling
PSO	Particle Swarm Optimization
PV	Photovoltaic
RE	Renewable Energy
SC	Supercapacitor
SG	Smart Grid
SSA	Sources Sizing Algorithm
UG	Utility Grid
V2G	Vehicle to Grid
WT	Wind Turbine

THESIS ABSTRACT

NAME: Umer Akram

TITLE OF STUDY: JOINT CAPACITY OPTIMIZATION OF RENEWABLE GENERATION AND HYBRID ENERGY STORAGE FOR MICRO-GRIDS

MAJOR FIELD: Electrical Engineering

DATE OF DEGREE: November 2017

During the past few decades, rising concerns for global warming and volatile fossil fuels prices have made renewable energy (RE) sources an attractive alternative. This trend has been further underpinned by rapid advancements in the power electronics field, which enabled full controllability of RE sources, within the constraints inflicted by the natural phenomenon. However, higher cost and stochastic nature of intermittent RE resources complicates their planning, integration and operation in electric power system. RE sources technologies, i.e., solar photovoltaic (PV) panels and wind turbines (WTs) are dependent on the resources that are random, stochastic, and intermittent as they depend upon weather and climatic changes and time of the day and year. The design of a system employing RE sources and energy storage system (ESS) depends upon

the behavior of load, solar irradiation, and wind power. So, optimal capacities of RE sources and ESS calculated for a particular geographical location cannot be taken as optimal for any other location even with same value of peak load demand. Thus, to harvest maximum benefits it is necessary to optimize RE sources and ESS altogether. This work presents methodologies for the design of microgrids (MGs), employing both conventional and renewable distributed generators and energy storage systems, operated in both grid-connected and stand-alone modes. Solar photovoltaic (PV) panels, wind turbines (WTs), and diesel generators (DGs) are utilized for distributed generation and battery energy storage (BES) system and hybrid energy storage system (HESS) comprising of BES and super capacitor (SC) technology are utilized for energy storage purpose. The optimization problems are formulated, and they involve variety of realistic constraints from RE generation, DGs, ESS, and load and objective functions are proposed to (i) minimize the cost, (ii) improve the reliability, (iii) decrease greenhouse gases (GHG) emissions, and (iv) curtail dump energy. All the objectives have special significance in designing a MG, for example, cost is related to the economics, GHG emissions deal with global warming, and dump energy is related to the stability and economics of the system. The labyrinthine optimization problems are formulated and solved innovatively to decrease the complexity and computational time. As a case study, the proposed methodologies are validated using real-world data of wind speed, solar irradiation and power demand from Dammam city in Saudi Arabia. Simulation results show the effectiveness of the proposed methodologies. This study could be assumed as a powerful roadmap for decision makers, analysts, and policy makers.

ملخص الرسالة

الاسم الكامل: عمر أكرم
عنوان الرسالة: التحسين الأمثل للقدرة المشتركة لكل من التوليد المتجدد للطاقة و التخزين المهجن للطاقة في الشبكات المصغرة
التخصص: الهندسة الكهربائية
تاريخ الدرجة العلمية: نوفمبر ٢٠١٧

خلال العقود القليلة الماضية، جعلت المخاوف المتزايدة بشأن الاحتباس الحراري و الأسعار المتقلبة للوقود الأحفوري من مصادر الطاقة المتجددة (RE) بديلاً جذاباً. و قد تعزز هذا الاتجاه أكثر بسبب التقدم السريع في مجال إلكترونيات القوى – و التي مكنت من التحكم الكامل بمصادر الطاقة المتجددة – في حدود القيود التي تفرضها الظواهر الطبيعية. و مع ذلك، فإن التكلفة المرتفعة و الطبيعة العشوائية لمصادر الطاقة المتجددة و تقطعها تعقد عمليات التخطيط لتلك المصادر، و التكامل، و التشغيل في نظام الطاقة الكهربائية. تعتمد تقنيات مصادر الطاقة المتجددة، مثل الألواح الشمسية الكهروضوئية (PV) و توربينات الرياح (WTs)، على موارد ذات طبيعةٍ عشوائيةٍ، و تصادفيةٍ، و متقطعةٍ لأنها تعتمد على الطقس و التغيرات المناخية و على التوقيت اليومي و السنوي. فتصميم نظامٍ يوظف كلاً من مصادر الطاقة المتجددة و نظام تخزينٍ للطاقة (ESS) يعتمد على سلوك الحمل، و على الإشعاع الشمسي، و على طاقة الرياح. لذلك، فإن القدرة المُثلى لمصادر طاقةٍ متجددةٍ و نظام تخزينٍ للطاقة المحسوبة لموقعٍ جغرافيّ معينٍ لا تُعتبر مُثلى لأيّ موقعٍ آخر حتى لو تساوت قيم الحمل الأعلى. و بالتالي، فإن من الضروري تحسين مصادر الطاقة المتجددة مع نظام تخزين الطاقة لحصد أكبر قدرٍ من المنافع. يعرض هذا العمل منهجياتٍ لتصميم شبكاتٍ مصغرةٍ (MGs) – التي تستخدم مولداتٍ تقليديةٍ و مولداتٍ موزعةٍ للطاقة المتجددة و نظم تخزينٍ للطاقة – تعمل في كلا الوضعين: وضع الاتصال بالشبكة و الوضع المستقل. تستخدم الألواح الكهروضوئية (PV) و مولدات الرياح (WTs) و مولدات الديزل (DGs) في التوليد الموزّع للطاقة، و يستخدم نظام تخزين الطاقة الهجين (HESS) المكون من بطاريات تخزين الطاقة (BES) و تقنية المكثفات الفائقة (SC) لغرض تخزين الطاقة. تمت صياغة معادلات التحسين الأمثل، و التي اشتملت على مجموعةٍ متنوعةٍ من القيود الواقعية المستمدة من توليد الطاقة المتجددة و مولدات الديزل و نظم تخزين الطاقة و الأحمال، و وُضعت دوالّ الهدف من أجل: ١) تقليل التكلفة، ٢) تحسين الموثوقية، ٣) خفض انبعاثات الغازات الدفيئة (GHG)، ٤) الحد من الطاقة المهدرة. جميع الأهداف لها أهميةٌ خاصةٌ في تصميم الشبكة المصغرة، فعلى سبيل المثال: التكلفة مرتبطةٌ بالاقتصاد، و انبعاثات الغازات الدفيئة متعلقةٌ بالاحتباس الحراريّ، و الطاقة المهدرة مرتبطةٌ باستقرار و اقتصاديات النظام. تمت صياغة معادلات التحسين الأمثل المتاهية و حلُّها بصورةٍ مبتكرةٍ لتقليل التعقيد و الوقت الحسابيّ. كدراسة حالة، تم التحقق من المنهجيات المقترحة باستخدام بياناتٍ حقيقيةٍ لسرعة الرياح، و الإشعاع الشمسيّ، و الطلب على الطاقة في مدينة الدمام في المملكة العربية السعودية. أظهرت نتائج المحاكاة فعالية المنهجيات المقترحة. تُشكل هذه الدراسة خارطة طريقٍ قويةً لصناع القرار، و المحللين، و المشرّعين.

CHAPTER 1

INTRODUCTION

Most recently, major proportion of electricity is being produced by utilizing fossil fuels such as coal, natural gas and oil which emits massive amount of greenhouse gases in the environment. Moreover, fossil fuels reserves are depleting and their prices are also volatile. On the other hand, load demand is increasing and new environmental policies are also being legislated to curtail greenhouse gases emissions. For instance, 160 countries around the world have signed the Paris agreement to combat against the climate changes. To fulfill the agreement, nations around the globe are planning to reduce their greenhouse gases emissions, e.g., Kingdom of Saudi Arabia has planned to reduce CO_2 emissions by 130 million tons a year by 2030. So, a reduction in utilization of the fossil fuels and search for their substitutes is crucial for reliable and eco-friendly electricity generation. Renewable energy (RE) sources can be used as a substitute of the fossil fuels as they generate green energy and freely available in large abundance. The integration of RE sources in electric power grid has evolved into the concept of microgrid (MG). MGs are state-of-the-art active distribution networks consisting of distributed generators, energy storage system (ESS), and flexible loads, operated grid-connected or islanded, in a controlled, coordinated way [1, 2]. Due to the propinquity of distributed generators to the loads in MGs and the utilization of RE sources, MGs are trusted to supply its customers with more efficient and eco-friendly energy, reduced power losses and network congestion, and improved power quality and reliability compared to the energy supplied by conventional power plants [3–5]. MGs are contemplated to be an integral part of smart grids (SGs) in the future electric power system [6].

Solar and wind are two expeditiously emerging RE sources, especially solar has gained more popularity due to significant decline in its cost over the past few years [7, 8]. Since, such sources are intermittent, uncontrollable, stochastic, and highly variable, their integration in the electric power grid poses challenges to its effective operation, especially at higher penetration levels [9–11]. For example, load mismatch, poor load following, voltage instability, frequency deviation, inferior power quality, and reliability problems are some of the detrimental impacts that RE sources introduce in electric power network [12]. Now, innovative technologies and novel ideas are required to alleviate the aforementioned problems, to increase the penetration of RE sources in the electric power grid.

A potential candidate solution to the aforesaid problems is to store energy during surplus generation hours using ESS and redispatch it appropriately later when needed [13–17]. Several types of ESS are available and among them battery energy storage (BES) system is most frequently utilized [18–20]. It is also important to note that the cost of a MG employing RE sources and BESS is higher and too high cost is not acceptable. In the first part of this thesis a methodology for the capacity optimization of a MG employing RE sources and BESS system is developed so that it has lower cost and higher reliability.

Batteries are only efficient at supplying low steady loads, while outputs of RE sources are highly fluctuating, which are not suitable for them. It is difficult for batteries to recover from rapid power swings without a significant reduction in their lifetime [21]. An ideal ESS must have a high power density to follow rapid power fluctuations, a

high energy density to give autonomy to the electric power grid, and longer life. As a sole energy storage technology is unlikely to deliver these essentials effectively and economically, it is vital to couple multifarious energy storage technologies, creating a hybrid energy storage system (HESS) [22–24].

Most recently, HESS has become an emergig storage technology as it combines the benefits of multiple technologies. For example, BES and SC can be combined to build HESS [25–27]. The BES systems have high specific energy, low specific power, low self-discharge, low cycle life, long charge times, and relatively lower cost per watt-hour. On the other hand, the SC storage systems have low specific energy, high specific power, high cycle life, very high self-discharge, short charge times, and high cost per watt-hour [28, 29]. The HESS makes use of complementary properties of BES and SC and provides large energy supply, high power, and fast dynamic response at the same time economically and effectively [30–33]. Nevertheless, to optimize the lifetime of both BES and SC, it is vital to ensure that both operate within their operational constraints. BES must operate within its state of charge and current bounds and SC within its voltage and current bounds. At the same time the SC should respond to rapid large current signals in order to maximize the lifespan of BES [34, 35]. It is also important to note that the cost of energy storage units per kilowatt is a strong function of their capacity, and too high cost is prohibitive to commercial and industrial acceptance, a method for optimizing the size and operation of such HESS to fit application constraints is a crucial task. In the second part of this work, BES and SC storage technologies will be combined to build up a HESS as shown in Fig. 1.1. In the second part of this work

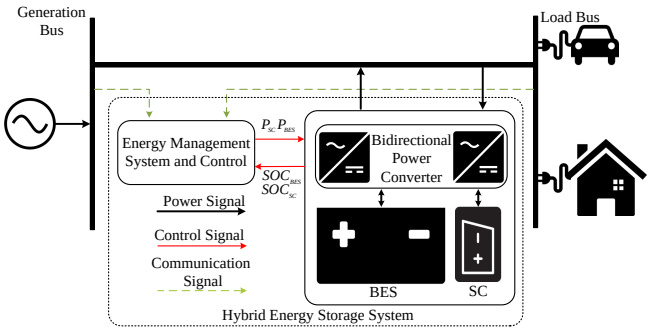

Figure 1.1: A hybrid energy storage system.

a methodology for the capacity optimization of grid-connected MG utilizing WT, PV, BES system and SC is developed.

Isolated and remote areas where supplying electricity through national grid is infeasible due to techno-economic constraints, standalone MG utilizing local available RE sources is considered as a viable attractive alternative and thus adopted in many regions and countries [36–39]. It is important to note that the cost of BES system is high, and has limited number of life cycles, so supplying a load at 100% reliability by utilizing RE sources and BES system only may result in very high cost. So, a dispatchable source, i.e., diesel generator (DG) should also be utilized along with the RE sources and BES system to supply a load more effectively and economically [40, 41].

Power output of DG is predictable and independent of climate. However, the use of DG has some disadvantages such as, environmental pollution by greenhouse gases (GHG) emissions and higher operation and maintenance costs. On the other hand, RE sources and BES system have high initial investment cost, negligible operation and maintenance costs and produce negligible GHG emissions. As too high cost and GHG emissions are prohibitive to commercial and industrial acceptance. So, developing a method for optimizing the sizes and operation of a system, utilizing RE sources, BES

system, and DG, to fit application constraints is a crucial task.

Transportation sector has been one of the major contributors of the GHG emissions [42–44]. The conventional vehicles use fossil fuels, i.e., diesel or gasoline, and emit gases such as carbon dioxide, carbon monoxide, hydrocarbons, and nitrogen oxides. Electric vehicles (EVs) have gained significant attention since the last decade as one of the promising solution for GHG emissions reduction [45]. Continuous advancements in EVs anticipate their massive penetration in the future power system, and the typical load diagram of future power system can be significantly different from the present one without EVs [46, 47]. Hence, substantial number of EVs must be considered for future power system planning to ensure the customers daily travel.

MGs are envisaged to be transformed to SGs in the future electric power system due to, the innovations in power electronics, and the introduction of the advance high-speed information and communication systems and sophisticated control [48–50]. SGs are perceived as next-generation power systems, provide two-way communication channels between power generation station and the end user [51], and allow the shifting of load demand away from peak load hours or to renewable generation periods, thereby improving reliability and stability, increasing efficiency, reducing the capacity of peaking generation, which consequently results in several financial, technical, and environmental benefits [52–54]. Moreover, the recent increase in the usage of EVs will significantly intensify the load demand, yet at the same time this will improve the pliability of load demand by the control of EVs charging periods and vehicle-to-grid operations [55, 56]. Owing to these facts, the planning, design, operation, and management of the next-

generation power system will not be alike the conventional power system, where all of the involved technologies should be contemplated at the planning and design stage. In the third part of this work a methodology for the capacity optimization of a standalone MG employing PV, WT, BES, and DG to supply a remote community power demand comprising of typical residential load demand and EVs load.

CHAPTER 2

LITERATURE REVIEW

The literature reporting the capacity optimization of RESs, can be divided in two main classes. The first class discusses the sizing of RESs and/or ESSs without considering the smart control of the load demand, and it has acquired much attention in the literature. Reference [57] has proposed a capacity optimization methodology for system employing PV, WT and BES system. The proposed technique is based upon the following key principles: i) high supply reliability, ii) complete usage of the complementary attributes of solar and wind, iii) less fluctuations in the power supplied to the utility grid, iv) BES system charge discharge rate optimization, and v) minimization of the total cost. The sizing of a system utilizing PV, WT, DG, BES system, fuel cell (FC), electrolyzer and hydrogen tank is done in [58]. A multi-objective cost function is developed with the aim of cost minimization, GHG emissions reduction, minimization of unmet load. Particle swarm optimization based approach has been used to solve the multi-objective optimization problem. A multi-criteria decision-making algorithm is presented in [59] for capacity optimization of a PV, WT system, that meets a certain balance of economic, environmental, and social factors. A multi-objective optimization algorithm is developed in [60] for the sizing of a standalone system employing PV, WT, BES system. The sizing is done based upon the power supply reliability, the energy stability, the energy utilization ratio, and the economic efficiency. The non-dominated sorting genetic algorithm (GA) is used to determine the optimal sizes of a standalone system employing PV, WT, and BES system [61]. A optimization problem is solved to achieve minimum cost and maximum reliability. In [62], the capacity optimization of standalone system utilizing, PV, WT, BES system and DG is done based

upon three objectives, i.e., i) cost minimization, ii) job creation maximization, and iii) human development index maximization. A pareto-optimization multi-objective evolutionary algorithm is used to solve the optimization problem. The planning of PV, WT, and BES grid-connected MG is done based upon cost minimization and customer satisfaction maximization, and the optimization problem is solved using mixed integer linear programming [63]. In [64], sizing of PV and BES system is done with the aim of minimization of levelized cost of energy. The proposed methodology also aims to maximize the PV size. A robust optimization approach is proposed in [65] to determine the sizes of PV, WT, ESS supplying energy to a remote telecommunication facility. The aim of the optimization is to minimize the total cost and optimization is carried out as robust mixed-integer linear programming. A methodology for the capacity optimization of a standalone system utilizing PV, WT, BES system, and DG is developed in [66]. GA is used to solve the optimization problem to minimize the life cycle cost, reduce GHG emissions and reduce dump energy. In [67], PSO and fuzzy logic are used to determine optimal sizes and types of distributed generators and optimal capacity of ESS. In [68], sizing of PV, WT, and ESS is done based on minimization of total planning cost. In [69], sizing of WT, PV, BES, and FC is done based on the cost and reliability. In [70], optimal sizes of PV, WT, DG, BES, and pumped storage are determined based upon minimizing both initial investment and operational/maintenance costs. In [71], optimal sizing of MG comprising of WT, PV, BES, and biomass is done considering two alternative objectives, i.e., minimization of total annual energy losses and cost of energy. In [72], optimal sizing and sitting of renewable DGs is done based upon the

minimization of annual investment cost and operation cost. In [73], capacity optimization of PV and BES is done based upon levelized cost of energy. In [74], capacity optimization of PV, WT, tidal turbine, and BES is done based upon the net present cost and reliability, the optimization problem is solved using crow search algorithm. In [75], optimal sizes of PV, WT, diesel generator, biodiesel generator, FC, and BES are determined based on minimization of cost of energy. In [76], optimization of BES-SC is done based upon initial investment cost and simulated annealing PSO is used to solve the optimiztion problem. In [77], a statistical approach is used to optimize the size of the BES-SC hybrid storage system. In [78], an iterative technique based upon minimization of total annual cost is proposed for sizing of a standalone PV, WT and BESS system. In [79], optimal sizing of hybrid PV-WT generation system is done based upon the reliability and cost. In [80], optimal sizes of PV, WT and BESS are determined based upon cost, reliability and emissions, and well known optimization technique, i.e., particle swarm optimization (PSO) (see [81] for PSO) is used to solve the optimization problem. In [82], optimal sizes of PV, WT and BESS are determined based on minimizing the gap between load and demand. In [83], optimal sizing of PV, WT and BESS is done based upon the minimization of total present cost. In [84], a methodology for capacity optimization of RE sources and ESS is proposed based upon the minimization of initial investment and operation/maintenance costs. In [**?**], sizing of standalone MG system employing PV and BESS is done based upon the levelized cost of energy. In [85], authors have proposed a program that uses the GA for capacity optimization and operation control of a PV, DG system. The program has been devel-

oped in C++. In [86], authors have developed a sizing methodology based upon GA for a stand-alone hybrid PV-WT generation system utilizing BES for energy storage. The proposed technique can attain the required loss of power supply probability with a minimum cost of system. In [87], authors have developed a methodology for sizing of a stand-alone PV-BES system for remote areas in Sohar, Oman. The system design is based upon the cost. In [88], an economic evaluation of a PV-WT-FC generation system is performed for a home in the Pacific Northwest. In this design the combination of hydrogen storage tanks, an electrolyzer, and FC stack, is used as the ESS. Simulated annealing algorithm is used for capacity optimization of a PV-WT hybrid energy system integrated with BES in [89]. The proposed method uses a stochastic gradient search to determine the global optima. In [90], a modified PSO algorithm is used for capacity optimization of a hybrid PV-WT-FC generation system to supply of the demand reliably. The proposed design is based upon the minimization of annualized cost of the system over its period of operation. In [91] authors have investigated the performance of several variants of PSO algorithm on the capacity optimization problem of PV-WT-BES systems. The optimal system size has been evaluated under different performance modes using real-time information and meteorological data. In [92], authors have used the PSO algorithm for optimal sizing of a stand-alone hybrid PV-WT generation system. The study is performed for Kahnouj area in Iran. In [93], authors have presented an optimized design of MG in distribution systems with number of distributed generators under several market policies such as pool/hybrid electricity market. The proposed MG utilizes PV, WT, and BESS. The PSO technique is used to determine the optimal

design based upon cost. A discrete simulated annealing algorithm is used for capacity optimization of hybrid PV-WT generation system in [94]. The proposed algorithm is then expanded by using harmony search algorithm and chaotic search algorithm. A method based upon iterative technique is developed in [95] for capacity optimization of a stand-alone PV-WT-hydrogen system which supply power to a desalination unit. The proposed technique aims at determining the optimized technicaleconomic configuration of the set of system components. In [96], ant colony optimization is used for sizing of a hybrid PV-WT generation system. The system design is based upon the total cost. The capacity optimization of a hybrid PV-BES-DG system are performed by [97] for the remote locations in India, using artificial intelligence techniques without the metrological data. A methodology for optimization of a PV-WT-BES system for a specific location employing an iterative scheme has been addressed by [98]. Similarly, the capacity optimization of RE sources and ESS is discussed in [99–121].

The second class considers the integrating RESs in SG paradigm, where the potential role controllable loads, i.e., EVs and conventional loads for accommodating higher levels of sustainable energy sources are accentuated, for example in [122–128]. A stochastic method based upon monte-carlo simulation and particle swarm optimization is developed in [122] for the capacity optimization PV, WT and BES system supplying a smart household load. In [123] a stochastic based optimization methodology is presented for the sizing of PV, WT, BES system. Load shifting plans are developed to give some flexibility and decrease the mismatch between the generation and air conditioning and heating ventilation loads. The optimization problem is solved with the

aim of the cost minimization. The effect of several EV control strategies on reducing surplus generation and GHG emissions is studied in [124]. The effects of EVs on high PV penetration levels are investigated in [125]. In [128], the capacity optimization of grid-connected PV, WT and BES system is done based upon the cost minimization.

It is important to understand that the design of a system employing RE sources and ESS depends upon the behavior of load, solar irradiation, and wind power. It varies from one location to another depending on the local available resources. So, optimal capacities of RE sources calculated for a specific geographical location cannot be taken as optimal for any other location even with same value of peak load demand. Similarly, optimal size of ESS determined for a particular geographical location cannot be considered as optimal for any other location even with same installed capacities of RE sources. Thus, to harvest maximum benefits it is necessary to optimize RE sources and ESS altogether. Moreover, initial investment cost, operation and maintenance cost, replacement cost, reliability, GHG emissions, and dump energy should be considered in the objective function to get more optimized results. It is clearly evident from the existing literature, the researchers have considered cost and GHG emissions in their formulations. The dump energy that has special significance in the design of RE sources based system is ignored in most of the cases. Ignoring the dump energy at the design stage may lead the system towards the instability especially when the system is stand-alone. We believe that the three main important objectives that should be considered while designing RE based system are i) cost, ii) GHG emissions, iii) dump energy. The cost accounts for the economics, GHG emissions account for environmental policies,

and dump energy accounts for stable design and economics. Moreover, a new load type, i.e., EV load has not been considered and modeled properly for the planning of the future power systems. Moreover, the literature deals with the capacity optimization of MGs employing single or multiple RE sources, conventional DGs, ESS, and variety of loads, operating in grid-connected or islanded mode based upon cost or cost-reliability or cost-GHG emissions. And to date, to the best knowledge of authors no methodology has been developed for the joint capacity optimization of the emerging hybrid PV-WT and ultramodern BES-SC system employed by a grid-connected MG system.

CHAPTER 3

OPTIMAL SIZING OF A WIND/SOLAR/BATTERY HYBRID GRID-CONNECTED MICROGRID SYSTEM

3.1 Introduction

Higher cost and stochastic nature of intermittent renewable energy (RE) resources complicates their planning, integration and operation in electric power system. Therefore, it is critical to determine the appropriate sizes of RE sources and associated energy storage for efficient, economic and reliable operation of electric power system. In this chapter, two constraint-based iterative search algorithms are proposed for optimal sizing of wind turbine (WT), solar photovoltaic (PV) and battery energy storage system (BESS) in grid-connected configuration of a microgrid. The first algorithm, named as Sources Sizing Algorithm (SSA), determines the optimal sizes of RE sources while the second algorithm, called as Battery Sizing Algorithm (BSA), determines the optimal capacity of BESS. These algorithms are mainly based upon two key essentials, i.e., maximum reliability and minimum cost. The proposed methodology aims to avoid over- and under-sizing by searching every possible solution in the given search space. Moreover, the proposed methodology considers the forced outage rates of PV, WT and utilization factor of BESS which makes it more realistic. Simulation results depict the effectiveness of the proposed approach.

The remainder of the chapter is organized as follows. Section 2 defines the problem description while Section 3 presents the structure and mathematical modelling of the grid-connected MG. Section 4 discusses the proposed methodology. Section 5 contains results and discussions while conclusion is given in Section 6.

3.2 Problem Description

Most of the conventional power generating stations utilize fossil fuels to supply the load demand. These power stations have a major role in global warming. In addition, legislation for reduction of greenhouse gases impels the utilities to shift their generation from fossil fuels to renewables. High cost, low efficiency, intermittent nature and less controllability limit the utilization of renewables. Moreover, storage system is also required for reliable operation of RE sources. The advantages of both conventional and RE sources can be combined by integrating RE sources with the conventional grid. However, sizing of RE sources and BESS in a grid-connected system is essential for reduction of emissions at a reasonable cost.

Block diagram of the proposed methodology for optimal sizing of grid-connected MG is shown in Fig. 3.1. Initially, the MG is assumed to be in standalone mode for optimal sizing of PV, WT and BESS. The problem is divided into two steps, i.e., sources sizing and storage sizing. Sources Sizing Algorithm (SSA) first forms a search space by using wind power, solar power and demand data and then reduces it based on given constraints. Whereas, Battery Sizing Algorithm (BSA) finds the optimal capacity of BESS in terms of energy (MWh) and power (MW) for the reduced search space. The

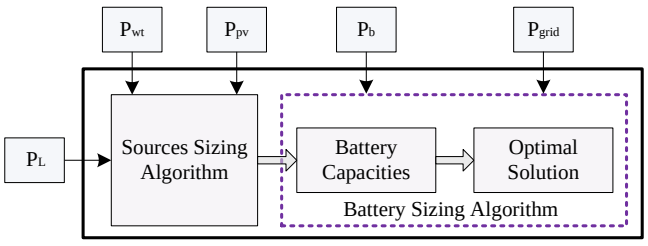

Figure 3.1: *The block diagram of the optimization algorithm*

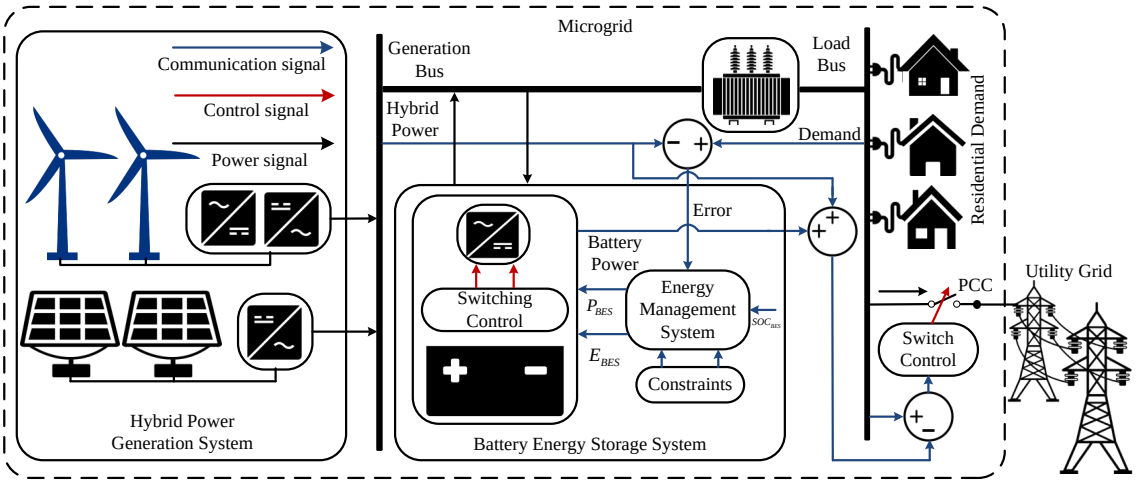

Figure 3.2: *A grid-connected MG system*

BSA determines the optimal solution based on reliability to cost ratio.

3.3 Microgrid Modelling

In this study, a grid-connected MG is shown in Fig. 3.2. Both WT and PV are utilized for hybrid renewable power generation while battery technology is employed for storage of electrical energy. A hybrid PV-WT generation topology utilizes both solar and wind to harvest maximum of the available energy. In addition, it is more reliable and efficient and requires less storage capacity than solar or wind alone making it more economical. The WT and PV are connected to generation bus via AC/AC and DC/AC converters respectively. However, BESS is connected to generation bus via bidirectional DC/AC converter. The load bus is connected to generation bus via transformer. The utility grid is also connected to load bus via controlled switch.

3.3.1 Wind Power System

A wind power system converts the kinetic energy of wind to electrical energy. Hourly wind speed can be estimated using Weibull distribution function [129].

$$F(v) = 1 - exp\left(-\left(\frac{v}{c}\right)^{\sigma}\right) \tag{3.1}$$

$$v = c\left[-ln(1-r)\right]^{\frac{1}{\sigma}} \tag{3.2}$$

$$v = c\left[-ln(r)\right]^{\frac{1}{\sigma}} \tag{3.3}$$

where σ is scale factor, c is shape factor, r is uniform random number and v is wind speed. The values of shape and scale factors of Weibull distribution function can be obtained from historical data. The monthly shape and scale factors of Dammam region are shown in Table 3.1. Output power of WT can be calculated using following equation [130]

$$P_{WT}(v) = \begin{cases} 0 & v < v_{ci} \\ P_{rated} \times \frac{v - v_{ci}}{v_r - v_{ci}} & v_{ci} \leq v < v_r \\ P_{rated} & v_r \leq v < v_{co} \\ 0 & v \geq v_{co} \end{cases} \tag{3.4}$$

Table 3.1: Monthly Shape and Scale Factors

Month	σ	c
Jan	2.40	4.77
Feb	2.45	4.85
Mar	2.55	5.15
Apr	2.40	5.06
May	2.40	5.52
Jun	2.60	6.51
Jul	2.50	5.54
Aug	2.30	4.91
Sep	2.20	4.18
Oct	2.05	4.09
Nov	2.20	4.38
Dec	2.00	4.68

where P_{rated} is the rated power of WT, P_{WT} is the power output of WT, v_r is rated speed, v_{ci} is cut-in speed and v_{co} is cut-out speed. The cut-in speed is the minimum speed required by WT to generate power. However, cut-out is the maximum speed allowed for power generation beyond which WT is shutdown to avoid damage. From (3.4) WT generates rated power between v_r and v_{co} whereas the power output increases linearly with speed between v_{ci} and v_r.

3.3.2 Solar Power System

A solar PV system harvests electrical energy from solar energy. Power output of PV module depends upon area of PV module, solar irradiation, atmospheric temperature and efficiency of PV module. In order to extract the maximum power, it is assumed that a maximum power point tracker is installed. The maximum hourly power output is calculated using the following equation [131]

$$P_{PV}(t) = \eta_{PV} A I(t) (1 - 0.005 (T_o(t) - 25)) \quad \forall t > 0 \tag{3.5}$$

where A is the area of solar cell array in m^2, η_{PV} is the efficiency of PV array, I is the solar irradiation in W/m^2 and T_o is the atmospheric temperature in ^oC.

3.3.3 Battery Energy Storage System

The battery energy storage system is composed of series and parallel strings of batteries. The state-of-charge of BESS at any instant of time is calculated as follows [132]

$$E_B(t) = E_B(t-1) + \eta_B \times \sum \{E_G(t) - E_L(t)\} \quad \forall t > 0 \tag{3.6}$$

subjected to following constraint

$$(1 - DOD) \leq E_B(t) \leq 1 \quad \forall t > 0 \tag{3.7}$$

where η_B is the charge/discharge efficiency, DOD is depth of discharge, E_B is the energy of BESS, E_G is the energy supplied by both RE sources and BESS and E_L is the load energy demand.

3.3.4 Grid Model

As mentioned earlier, output power of RE sources is sporadic, so a condition can arise during which output power of the RE sources and BESS becomes inadequate to supply the required load demand. During such events utility grid acts as backup and sells

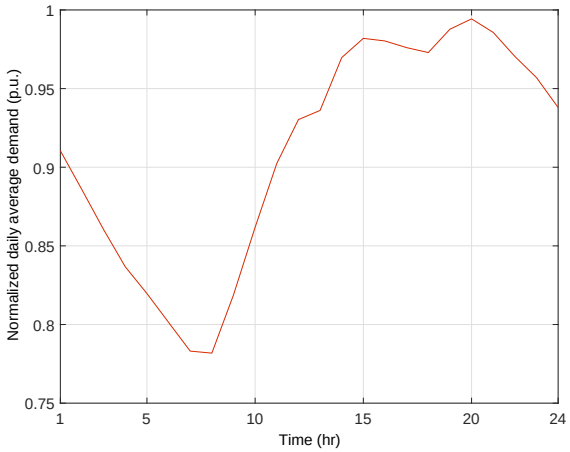

Figure 3.3: *Normalized average daily load demand of Dammam of calendar year 2015*

power to MG in order to meet the demand. The power supplied by the utility grid is modelled as follows

$$P_{grid}(t) = P_L(t) - \sum (P_{WT}(t), P_{PV}(t), P_{BES}(t)) \tag{3.8}$$

where P_{grid} is the power supplied by utility grid, P_L is the load power demand and P_{BES} is the power supplied by BESS.

3.3.5 System Demand

Dammam city lies in Eastern province of Saudi Arabia. Residential load demand of this city is used to test the proposed methodology. The normalized daily average demand of Dammam KSA in year 2015 is shown in Fig. 3.3. The minimum average daily power demand occurs from 6 am to 8 am, and it increases afterward, and peak power demand appears at 8 pm. It should be noted that the residential load demand data is considered that is why peak load demand occurs in the evening.

3.4 Proposed Methodology

The proposed methodology is divided into two sections. The first section discusses the sizing of RE sources, i.e., solar PV and WT using the SSA. While the section two determines the optimal capacity of BESS, i.e., MW and MWh and the optimal solution using the BSA.

3.4.1 Sources Sizing Algorithm

The hybrid power generated by a MG utilizing solar PV and WT is modelled as follows

$$P_G^{(i,j)}(t) = N_{PV}^i P_{PV}(t) PV_{status}^i(t) + N_{WT}^j P_{WT}(t) WT_{status}^j(t) \tag{3.9}$$

$$\forall i \in [1, i_{max}], j \in [1, j_{max}], t > 0$$

where

$$PV_{status}^i(t) = \begin{cases} 0 & G_{PV}^i(t) < FOR_{PV} \\ 1 & otherwise \end{cases} \quad \forall t > 0 \tag{3.10}$$

where

$$G_{PV}^i(t) = rand()$$

and

$$WT_{status}^j(t) = \begin{cases} 0 & G_{WT}^j(t) < FOR_{WT} \\ 1 & otherwise \end{cases} \quad \forall t > 0 \tag{3.11}$$

where

$$G_{WT}^{j}(t) = rand\,()$$

subjected to following capacities constraints

$$N_{PV}^{min} \leq N_{PV}^{i} \leq N_{PV}^{max} \tag{3.12}$$

$$N_{WT}^{min} \leq N_{WT}^{i} \leq N_{WT}^{max} \tag{3.13}$$

where P_G is the hybrid power generated by PV-WT system, N_{PV} and N_{WT} are the number of PVs and WTs, P_{PV} and P_{WT} are the powers generated by single PV and WT, PV_{status} and WT_{status} are the statuses of PVs and WTs which decide whether they would generate power or not. When the value of PV_{status} of a solar PV is 0 that means the solar PV cannot generate power because of some fault or any other reason. As given in (3.10) and (3.11), the values of PV_{status} and WT_{status} are calculated using the forced outage rates FOR_{PV} and FOR_{WT}. G_{PV} and G_{WT} are the random numbers which are generated using $rand()$ command of MATLAB. N_{PV}^{min}, N_{WT}^{min}, N_{PV}^{max} and N_{WT}^{max} are the minimum and maximum number of PVs and WTs which are calculated using following relations:

$$N_{PV}^{min} = \frac{\sum_{t=1}^{n} \alpha P_L\,(t)}{\sum_{t=1}^{n} P_{PV}\,(t)} \tag{3.14}$$

$$N_{WT}^{min} = \frac{\sum_{t=1}^{n} \beta P_L\,(t)}{\sum_{t=1}^{n} P_{WT}\,(t)} \tag{3.15}$$

$$N_{PV}^{max} = \frac{\sum_{t=1}^{n} \gamma P_L(t)}{\sum_{t=1}^{n} P_{PV}(t)} \tag{3.16}$$

$$N_{WT}^{max} = \frac{\sum_{t=1}^{n} \rho P_L(t)}{\sum_{t=1}^{n} P_{WT}(t)} \tag{3.17}$$

where α, β, γ and ρ are scaling factors and n is the total number of intervals. The instantaneous error/gap between load and generation is calculated as following

$$\Delta p^{(i,j)}(t) = P_L(t) - P_G^{(i,j)}(t) \quad \forall t > 0 \tag{3.18}$$

where Δp is the instantaneous error. The sum of absolute values of all instantaneous errors is referred as cumulative error ΔP and calculated as

$$\Delta P^{(i,j)}(t) = \sum_{t=1}^{n} \left(\left| \Delta p^{(i,j)}(t) \right| \right) \quad \forall t > 0 \tag{3.19}$$

where $\Delta P^{(i,j)}$ is the cumulative error corresponding to N_{PV}^{i} and N_{WT}^{j}. A smaller value of cumulative error reflects that the intermittent generation follows load demand effectively, while a larger value of cumulative error implies that there is a significant error/gap between hybrid renewable power generation and load demand. The cumulative error for every possible combination of PV and WT is calculated and stored in a matrix as follows

$$\boldsymbol{\Delta P} = \begin{bmatrix} \Delta P^{(1,1)} & \cdots & \Delta P^{(1,j_{max})} \\ \vdots & \ddots & \vdots \\ \Delta P^{(i_{max},1)} & \cdots & \Delta P^{(i_{max},j_{max})} \end{bmatrix}_{(i_{max} \times j_{max})} \tag{3.20}$$

where $\boldsymbol{\Delta P}$ is the error matrix that contains the values of all possible cumulative errors. The values of N_{PV} and N_{WT} that correspond to each cumulative error are stored in the vectors $\mathbf{N_{PV}}$ and $\mathbf{N_{WT}}$ as

$$\mathbf{N_{PV}} = \begin{bmatrix} N_{PV}^{min} & \cdots & N_{PV}^{max} \end{bmatrix}^{T}_{(i_{max} \times 1)} \tag{3.21}$$

$$\mathbf{N_{WT}} = \begin{bmatrix} N_{WT}^{min} & \cdots & N_{WT}^{max} \end{bmatrix}_{(1 \times j_{max})} \tag{3.22}$$

A search space is generated using $\boldsymbol{\Delta P}$, $\mathbf{N_{PV}}$ and $\mathbf{N_{WT}}$

$$\mathbf{S_{space}} = \begin{bmatrix} 0 & \mathbf{N_{WT}} \\ \mathbf{N_{PV}} & \boldsymbol{\Delta P} \end{bmatrix}_{(i_{max}+1) \times (j_{max}+1)} \tag{3.23}$$

where $\mathbf{S_{space}}$ is the search space. The $\mathbf{S_{space}}$ contains all possible combinations of PV and WT and the cumulative errors that correspond to each combination. The $\mathbf{S_{space}}$ is reduced by choosing minimum value of ΔP from its each column. Mathematically

$$\mathbf{\Delta P_{min}} = \begin{bmatrix} \Delta P_{min}^{1} & \cdots & \Delta P_{min}^{j_{max}} \end{bmatrix}_{(1 \times j_{max})} \tag{3.24}$$

where

$$\Delta P_{min}^{j} = min\left(\mathbf{S_{space}}\left(z, j\right)\right) \quad \forall j \tag{3.25}$$

$$z = 2, ..., i_{max} + 1$$

where $\boldsymbol{\Delta P}_{min}$ is the vector which contains the minimum values (selected from the $\mathbf{S_{space}}$) of cumulative errors. The values of N_{PV} and N_{WT} that correspond to each ΔP_{min} are given as

$$\mathbf{N_{PV_{min}}} = \begin{bmatrix} N_{PV_{min}}^{1} & \cdots & N_{PV_{min}}^{j_{max}} \end{bmatrix}^{T}_{(j_{max} \times 1)} \tag{3.26}$$

$$\mathbf{N_{WT_{min}}} = \begin{bmatrix} N_{WT_{min}}^{1} & \cdots & N_{WT_{min}}^{j_{max}} \end{bmatrix}_{(1 \times j_{max})} \tag{3.27}$$

A reduced search space is generated using $\boldsymbol{\Delta P}_{min}$, $\mathbf{N_{WT_{min}}}$ and $\mathbf{N_{PV_{min}}}$ given below

$$\mathbf{RS_{space}} = \begin{bmatrix} \mathbf{\Delta P_{min}}^{T} & \mathbf{N_{PV_{min}}} & \mathbf{N_{WT_{min}}}^{T} \end{bmatrix}_{j_{max} \times 3} \tag{3.28}$$

where $\mathbf{RS_{space}}$ is the reduced search space. There are j_{max} combinations in $\mathbf{RS_{space}}$ for which there will be j_{max} optimal storage units, one for each combination. The SSA is explained in Algorithm I.

Algorithm I: Sources Sizing Algorithm

Initialization: $i \leftarrow 1$, $j \leftarrow 1$, $t \leftarrow 1$

- **Data Generation**

Read: c, σ, I, $Load$

Calculate: P_{PV}, P_{WT}, P_G, N_{PV}^{min}, N_{WT}^{min}, N_{PV}^{max}, N_{WT}^{max} (3.4), (3.5), (3.9), (3.14)-(3.17)

Save: P_{PV}, P_{WT}, P_L, N_{PV}^{min}, N_{WT}^{min}, N_{PV}^{max}, N_{WT}^{max}, P_G

- **Search Space Formation**

While $i \leq i_{max}$ **Do**

While $j \leq j_{max}$ **Do**

Calculate: $\Delta P^{(i,j)}$, $\boldsymbol{\Delta P}$ (3.18), (3.19)

Save: $\boldsymbol{\Delta P}$, $\mathbf{N_{PV}}$, $\mathbf{N_{WT}}$ (3.24)

Calculate: $\mathbf{S_{space}}$ (3.23)

$j \leftarrow j+1$

End While

$i \leftarrow i+1$

End While

- **Reduced Search Space Formation**

While $j \leq j_{max}+1$ **Do**

While $i \leq i_{max}+1$ **Do**

Calculate: ΔP_{min}^{j}, $N_{PV_{min}}^{j}$, $N_{WT_{min}}^{j}$ (3.25)

$i \leftarrow i+1$

End While

Calculate: $\mathbf{\Delta P_{min}}$, $\mathbf{N_{PV_{min}}}$, $\mathbf{N_{WT_{min}}}$

$j \leftarrow j+1$

End While

Calculate: $\mathbf{RS_{space}}$ (3.28)

3.4.2 Battery Sizing Algorithm

The power generated by case number u selected from $\mathbf{RS_{space}}$ can be calculated using following equation

$$P_G^u(t) = N_{PV_{min}}^u P_{PV}(t) + N_{WT_{min}}^u P_{WT}(t) \tag{3.29}$$

$$\forall u \in [1, j_{max}], t > 0$$

subjected to the following constraints

$$N_{PV_{min}}^1 \leq N_{PV_{min}}^u \leq N_{PV_{min}}^{j_{max}}$$

$$N_{WT_{min}}^1 \leq N_{WT_{min}}^u \leq N_{WT_{min}}^{j_{max}}$$

where P_G is the power generated by the PVs and WTs that are selected for $\mathbf{RS_{space}}$. The difference in generation and demand is calculated as follows

$$p_{gap}^u(t) = P_L(t) - P_G^u(t) \quad \forall u, t > 0 \tag{3.30}$$

where p_{gap} is the gap between generation and demand. The maximum capacity of BESS that can be employed to store all of the excess energy is determined by using the algorithm given below. This algorithm represents the operation of BESS based upon which maximum capacity, that can be installed, has been calculated.

$$P^u_{gap}(\hbar) = \begin{cases} P^u_{gap}(\hbar) & P^u_{gap}(\hbar) > 0 \\ & \forall \hbar > 0 \\ 0 & otherwise \end{cases} \tag{3.31}$$

where

$$P^u_{gap}(\hbar) = \sum_{t=1}^{\hbar} p^u_{gap}(t) \tag{3.32}$$

The maximum storage size required to store the maximum of the excess energy is calculated as

$$B^u_{max} = max\left(P^u_{gap}\right) \tag{3.33}$$

where B_{max} is the maximum energy capacity of the BESS. The required battery storage capacity is less than or equal to B_{max} which is calculated using following relation

$$B^u_{cap} = \begin{cases} B^u_{max} & x = 1 \\ CBS^u & x = 0 \end{cases} \tag{3.34}$$

where B_{cap} is referred as required energy capacity of BESS. The B_{cap} equals to B_{max} if the battery discharges fully after its full charging period, this condition is indicated by $x = 1$. The B_{cap} is equal to corrected battery size *CBS* if the battery does not discharge fully after its full charging period, this condition is indicated by $x = 0$. The condition $x = 0$ implies that the battery is over-sized. An iterative region reduction algorithm is used to calculate *CBS* which is given by following equations:

$$CBS^u(w) = \frac{S^u_{min}(w) + S^u_{max}(w)}{2} \tag{3.35}$$

where

$$S^u_{min}(w+1) = \begin{cases} S^u_{min}(w) & x = 1 \\ CBS(w) & x = 0 \end{cases} \tag{3.36}$$

and

$$S^u_{max}(w+1) = \begin{cases} S^u_{max}(w) & x = 0 \\ CBS(w) & x = 1 \end{cases} \tag{3.37}$$

$$STEP^u_a = S^u_{max}(w) - S^u_{min}(w) \tag{3.38}$$

where S_{min} and S_{max} are minimum and maximum boundaries of the solution, $STEP_a$ is the difference between the minimum and maximum boundaries and w is the iteration number. Initially S_{min} and S_{max} are set equal to 0 and B_{max} respectively. Both of them get updated in an iterative fashion until $STEP_a$ becomes less than or equal to the allowable tolerance e. The B_{cap} is the required size but it is not optimal. If it is installed, the system will be reliable but not efficient and economical.

An important parameter that is required to be checked is the utilization factor; a higher value of the utilization factor decreases idle time and guarantees maximum benefit from BESS. Therefore, utilization factor is used to determine the optimal capacity of BESS. To compute utilization factor, battery decision variable BDV is calculated as following

$$BDV^u = \frac{\sum B^u_{chg-dcg}(t)}{n} \quad \forall t > 0 \tag{3.39}$$

where

$$B^u_{chg-dcg}(t) = \begin{cases} 1 & |P^u_{gap}(t) - P^u_{gap}(t-1)| \geq \lambda P^u_{b_{max}} \\ & \forall t > 0 \\ 0 & else \end{cases} \tag{3.40}$$

where $B_{chg-dch}$ is the BESS charging/discharging factor, it equals to 1 when the charging/discharging power is $\geq \lambda P_{b_{max}}$, λ is a constant and its value is between 0 and 1. Finally, optimal energy capacity of BESS is calculated as following

$$B^u_{opt} = \begin{cases} B^u_{cap} & BDV^u \geq B_{lim} \\ BCS^u & else \end{cases} \tag{3.41}$$

where B_{opt} is the optimal energy capacity of BESS and B_{lim} is the minimum BESS utilization limit. The B_{opt} equals to battery corrected size BCS if BDV is less than B_{lim}, otherwise B_{opt} equals to B_{cap}. The BCS is determined using a region reduction iterative algorithm as given below:

$$BCS^u(w) = \frac{OCF^u_{min}(w) + OCF^u_{max}(w)}{2} \tag{3.42}$$

where

$$OCF^u_{min}(w+1) = \begin{cases} OCF^u_{min}(w) & BDV^u \geq B_{lim} \\ BCS^u(w) & else \end{cases} \tag{3.43}$$

and

$$OCF^u_{max}(w+1) = \begin{cases} BCS^u(w) & BDV^u \geq B_{lim} \\ OCF^u_{max}(w) & else \end{cases} \tag{3.44}$$

$$STEP_b^u = OCF_{max}^u(w) - OCF_{min}^u(w) \tag{3.45}$$

where $STEP_b$ is the error, OCF_{min} is lower boundary of solution while OCF_{max} is upper boundary of solution. Initially, OCF_{min} and OCF_{max} are set to 0 and B_{cap} respectively, both get updated in iterative fashion until $STEP_b$ becomes less than the allowable tolerance e. The process of calculation of B_{opt} is repeated for every selected combination of PV and WT.

Cost and reliability are two important parameters that can be used to assess the performance of a system. An electric power system having higher reliability (energy served) and lower cost can be considered to have better performance. The optimal solution in this study is determined on the basis of cost and reliability. The total generation after finding the suitable size of the BESS for combination number u is calculated as follows

$$P_{GT}^u(t) = N_{PV_{min}}^u P_{PV}(t) + N_{WT_{min}}^u P_{WT}(t) + P_{BES}^u(t) \tag{3.46}$$

where P_{BES} is the power supplied by BESS and P_{GT} is the total power generated by the MG. A reliability index, i.e., energy served, is the total demand that system serves during its operation.

$$E_S^u = \sum_{t=1}^{n} D(t)^u \tag{3.47}$$

where

$$D(t)^u = \begin{cases} P_L(t) & P_{GT}^u(t) \geq P_L(t) \\ & \forall t > 0 \\ P_{GT}^u & otherwise \end{cases} \tag{3.48}$$

where E_S is the energy served. Similarly, another important reliability index is energy not served and it is the sum of total demand that is not served by a system during its operation. Mathematically, energy not served is modeled as

$$E_{NS}^u = \sum_{t=1}^{n} G(t)^u \tag{3.49}$$

where

$$G(t)^u = \begin{cases} P_L(t) - P_{GT}^u & P_L(t) > P_{GT}^u \\ & \forall t > 0 \\ 0 & otherwise \end{cases} \tag{3.50}$$

where E_{NS} is energy not served. The present worth factor PWF to calculate the net discounted energy served can be defined as

$$PWF = \left[\frac{(1+d)^l - 1}{d\,(1+d)^l} \right] \tag{3.51}$$

and net discounted energy served is calculated as

$$NDE_S^u = E_S^u PWF \tag{3.52}$$

where NDE_S is the net discounted energy served, d is the discount rate and l is the year of operation. The total cost C_T is the sum of investment cost, operation/maintenance

cost and replacement cost.

$$C_T^u = C_c^u + C_{om}^u + C_{rep}^u \tag{3.53}$$

where C_c is the initial investment cost, C_{om} is operation/maintenance cost and C_{rep} is the replacement cost. The operation/maintenance cost consists of fixed and variable operation/maintenance costs. The economic data of RE sources and BESS is tabulated in Table reftab:tab1.2. The cost of generation is calculated as

$$C_g^u = \frac{\sum_{k=1}^{N} NPV_k^u}{NDE_S^u} \tag{3.54}$$

where C_g is the cost of generation of MG, NPV is the net present value of total cost. The optimal decision variable ODV is defined as follows

$$ODV^u = \frac{E_s^u}{C_g^u} \tag{3.55}$$

The solution vector is generated as

$$\mathbf{SV} = \begin{bmatrix} ODV^1 & \cdots & ODV^{j_{max}-1} & ODV^{j_{max}} \end{bmatrix}_{(1\times j_{max})} \tag{3.56}$$

where **SV** is the solution vector. There is an optimal combination of solar PV, WT and BESS capacities corresponding to every index of **SV**. While the optimal solution corresponds to the index of maximum value of the **SV**, as the maximum value of SV implies that the MG has higher reliability at a relatively lower cost. From (3.55) it seems that the value of ODV will also be maximum for lower cost and lower reliability, but in

fact for lower investments, i.e., for smaller capacities of PV, WT and BESS, the value of reliability is very small and with the increase in the investment cost, i.e., increasing the capacities of PV, WT, and BESS the percentage increase in the reliability is more as compared to percentage increase in the investment cost. The BSA is explained in Algorithm II.

Algorithm II: Battery Sizing Algorithm

Initialization: $u \leftarrow 1$, $t \leftarrow 1$, $e \leftarrow 0.1$

While $u \leq j_{max}$ **Do**

Calculate: P_G^u, p_{gap}^u, P_{gap}^u (3.29), (3.30), (3.31)

- **Required Battery Size**

Calculate: B_{max}^u, x (3.33)

If $x = 1$ **Do**

$B_{cap}^u \leftarrow B_{max}^u$

Else Do

Calculate: CBS^u (3.35)

$B_{cap}^u \leftarrow CBS^u$

End If

- **Optimal Battery Size**

Calculate: $B_{chg-dcg}^u$, BDV^u (3.39), (3.40)

If $BDV^u \geq B_{lim}$ **Do**

$B_{opt}^u \leftarrow B_{cap}^u$

Else Do

Calculate: BCS^u (3.42)

$B^u_{opt} \leftarrow BCS^u$

End If

Calculate: P^u_{GT}, E^u_S, C^u_g, ODV^u, **SV** (3.46), (3.47), (3.54), (3.55), (3.56)

$u \leftarrow u+1$

End While

Table 3.2: Economic data

Source Type	C_c ($/kWh*, $/kW)	C_M(fixed) ($/kWh/yr.)	C_M(variable) ($/kWh/yr.)	Life (yr.)
WT	2346	33	0	20
PV	2025	16	0	20
BESS*	450	10	0	10

3.5 Results and Discussions

The BSA has selected 1000 different possible combinations of PV and WT for reduced search space. The BESS capacity for each selected combination is calculated using the BSA. Solar PV, WT and BESS capacities combinations are shown in Fig. 3.4. As mentioned earlier, reliability and cost are the two main parameters that can be used to assess the performance of a MG. The BSA has carried out reliability and economic analyses of the combinations selected for reduced search space to determine the optimal solution. The **SV** as in (3.56) generated by the BSA is shown in Fig. 3.5. It is important to note that for each index of **SV** there is a combination of WT, PV and BESS, and overall installed capacities of RE sources and BESS increase with the increase in the index. The

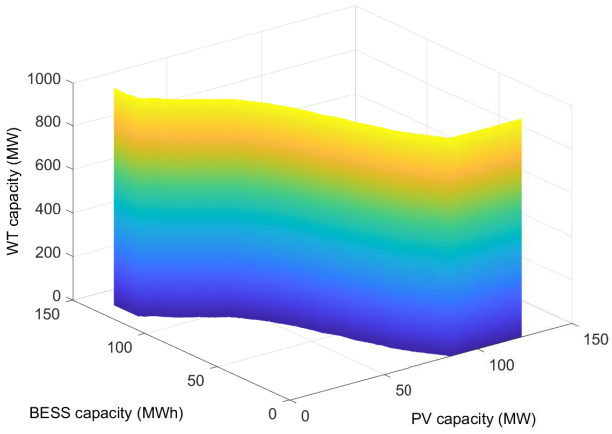

Figure 3.4: *Combinations of WT, solar PV and BESS capacities*

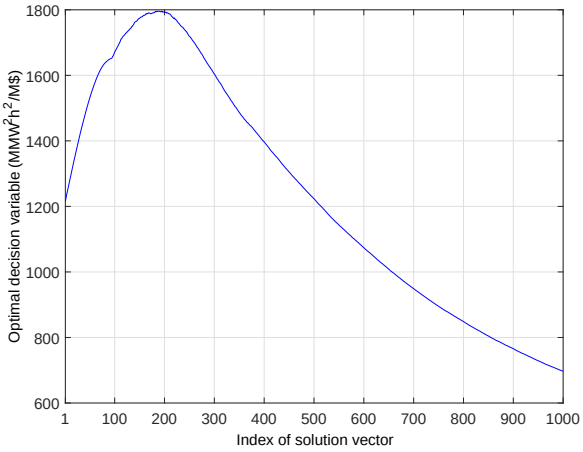

Figure 3.5: *Solution vector*

optimal combination corresponds to the index with maximum value of ODV. Because a higher value of ODV implies relatively higher reliability at a reasonable lower cost, while a smaller value of ODV shows higher reliability at a very high cost or low reliability at a lower cost. It can be observed from Fig. 3.5 that the combination of PV, WT and BESS corresponding to the index number 187 of the **SV** is the optimal solution. The capacities of the PV, WT and BESS are 57 MW, 187 MW and 63 MWh (20 MW) respectively.

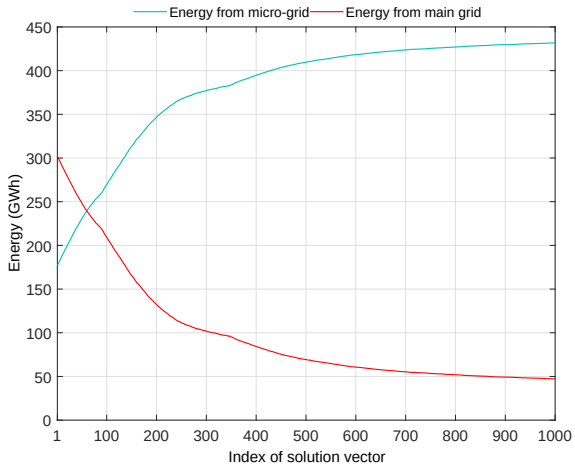

Figure 3.6: *Energy share of MG and main grid*

There is an increase at the beginning until the maximum point and then decreasing trend is observed for the values of *ODV*. Smaller values of *ODV* in the beginning are due to the fact that energy served is very little for smaller capacities of PV, WT and BESS. Similarly, values of *ODV* are also small for higher indices because for large installed capacities the cost becomes very high which makes the solution un-economical. Although, reliability (energy served) is also higher for larger capacities but its impact on *ODV* is non-dominant as compared to cost, as costs of RE sources and storage are high and for very large capacities overall cost becomes even more higher which makes the solution very expensive. Moreover, from Fig. 3.4 and Fig. 3.5 it can also be observed that appropriate limits of minimum and maximum capacities of PV and WT should be selected while determining the optimal size using any technique. The narrow limits may lead the algorithms to operate in the region where the values of *ODV*s are low and result in an un-economical solution.

As mentioned earlier, that output of the RE sources is intermittent, so during the operation of the MG it may happen that output of the MG becomes insufficient to meet

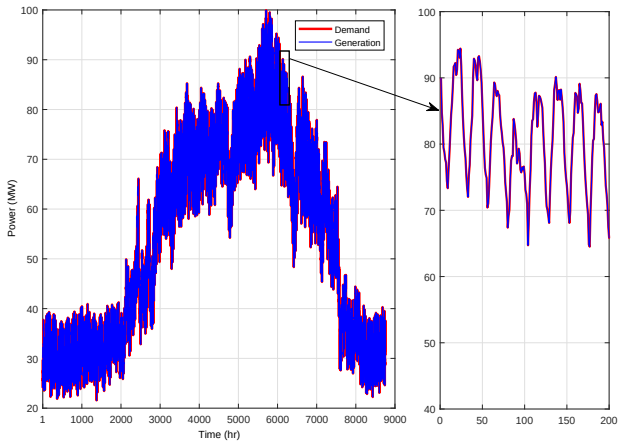

Figure 3.7: *The variation in generation and demand throughout the year*

the required demand, in such events, the MG buys power from utility grid to supply the load. Total energy served by the MG and utility grid to meet the required load is shown in Fig. 3.6. It can be seen that with the increase in indices the energy served by the MG increases while energy served by utility grid decreases. In the beginning, energy served by the MG rises and energy served by utility grid reduces rapidly and finally both saturate.

The variation in demand and generation throughout a year is shown in Fig. 3.7. It can be observed that the generation is always equal to the demand. As the system under study is grid-connected, and utility grid is serving as a backup. So, whenever the output power of MG becomes inadequate to supply the required load demand, MG buys power from the utility grid and in this way the generation remains always equal to demand making the overall system highly reliable.

To show that the global optimum can be reached, the sizing problem is formulated and solved using genetic algorithm also. The optimal capacities of PV, WT and BESS determined by genetic algorithm are 57.3 MW, 187 MW and 63 MWh. Hence,

Table 3.3: Comparison between different possible solutions

Case Index	PV (MW)	WT (MW)	BES (MWh)	BES (MW)	MG Energy (GWh)	Utility Energy (GWh)	MG Cost (c/kWh)	Total Cost c/kWh	CO_2 (kt)
CASE-I	-	-	-	-	-	478.8	-	10	527.77
CASE-II	82	100	53	17	268.9	210	15.91	13.32	231.65
CASE-III	57	187	63	20	339.3	139	18.73	16.18	153.33
CASE-IV	40	250	94	30	369.8	109	21.11	18.58	120.24
CASE-V	10	650	133	43	422.8	56	41.67	37.96	61.73

Table 3.4: Energy Supplied by PV-WT and BES System

Case Index	Energy supplied by PV-WT System (MWh)	Energy Supplied by BES System (MWh)
CASE-II	166.8	1102
CASE-III	239.72	99.6
CASE-IV	266.44	103.2
CASE-V	317.86	104.94

both algorithms have found the same solution, the small deviation in the size of PV is due to randomness factor. Although both algorithms resulted in the same solution but computational time of the proposed algorithm is lesser and guarantees global maxima. Moreover, unlikely to most of the conventional optimization algorithms, in the proposed algorithm user can visualize that how the solution is being determined, and user can communicate to the algorithm to determine the required solution in an easy and understandable way. Also, there is no parameter tuning involved in the proposed algorithm like the most of conventional optimization approaches, which are based upon hit and trial methods.

To show the effectiveness of the proposed methodology, a comparison based upon per unit cost, clean energy supplied (energy supplied by MG) and CO_2 emissions, between different possible solutions is presented in Table 3.4. The CASE-I represents that all energy is supplied by conventional generation system. The per unit cost is lowest while emissions are highest for this case. The remaining cases represent that energy is supplied by both MG and utility. The overall cost for CASE-II is reasonable and emissions are also moderate for this case. The clean energy served by CASE-III is more as compared to the CASE-II. We can see from Table 3 that while moving from CASE-II to CASE-III the percentage increase in the clean energy served is more as compared to the percentage increase in overall cost. Also, percentage decrease in CO_2 emissions is more as compared to percentage increase in cost. Hence, we can conclude that CASE-III is better than CASE-II. The CO_2 emissions of CASE-III are almost 70% less as compared to the CASE-I, i.e., conventional generation. The CO_2 emissions are lowest for CASE-V whereas per unit cost is very high for this case due to large installed capacities of RE sources and BESS. The overall cost per unit for CASE-IV is also high and CO_2 emissions are lower. It is clear from the above discussion that CASE-III is an optimal solution as it serves a considerable amount of clean energy and reduces CO_2 emissions by substantial amount at reasonable per unit cost, i.e., 16.18 c/kWh. It is important to note that the cost is the factor/function of many other parameters, for example, a location with higher correlation between the solar irradiation, wind speed curve and load curve would result in further reduction in cost, and our optimized solution will then be more effective and justified.

Table 3.4 shows the energy supplied by hybrid PV-WT system and BES system. It can be observed from the analysis of CASE-II, CASE-III and CASE-IV that the increase in RE installed capacities increases the contribution from renewables significantly, while the CASE-IV and CASE-V show that even a significant increase in RE installed capacities has a minor increase in the energy supplied by RE sources. This is due to he fact that by just increasing the installed RE capacity, the contribution from clean energy resources cannot be increased in reality, it may be because of higher generation than demand case; on the other hand sometimes cost goes higher than the revenue and hence further increasing the RE capacities does not affect the energy supplied or it may not be economical. This leads to the need of optimal capacity calculations.

MATLAB is used for the modelling and simulations. Core i7, 6th generation, 2.6 GHz, 16 GB RAM, platform is used to run the simulations.

CHAPTER 4

COMBINED CAPACITY OPTIMIZATION OF HYBRID WIND-SOLAR AND BATTERY-SUPERCAPACITOR MICROGRID SYSTEM

4.1 Introduction

This chapter presents a methodology for the joint capacity optimization of renewable energy (RE) sources, i.e, wind and solar, and state-of-the-art hybrid energy storage system (HESS) comprising of battery energy storage (BES) and supercapacitor (SC) storage technology, employed in a grid-connected microgrid (MG). The problem involves multiple fields, i.e., RE, battery technology, SC technology, and control theory, and requires an efficient and precise co-ordination between sub-fields to harness the full benefits, this makes the problem labyrinthine. The optimization problem is formulated, and it involves variety of realistic constraints from both hybrid generation and storage, and an objective function is proposed to (i) minimize the cost, (ii) improve the reliability, and (iii) curtail green house gases (GHG) emissions. The complex optimization problem is solved innovatively in piece-wise fashion to decrease the complexity and computational time. First, sizes of solar photovoltaic (PV) and wind turbine (WT) are determined using an innovative search algorithm, and in the second step, the size of HESS is calculated, finally the optimal solution is determined. A comparison based upon cost, reliability, and GHG emissions is presented which plainly shows the effectiveness of the proposed methodology. The technique is also applied to determine the size of a MG employing PV, WT and BES operating in grid-connected mode. And a brief cost analysis, reliability assessment, and emission reduction are given for three scenarios, 1) MG with HESS, 2) MG with BES, and 3) MG with conventional generation. It is shown that a MG with HESS is not only economical but also more reliable and has lower GHG emissions.

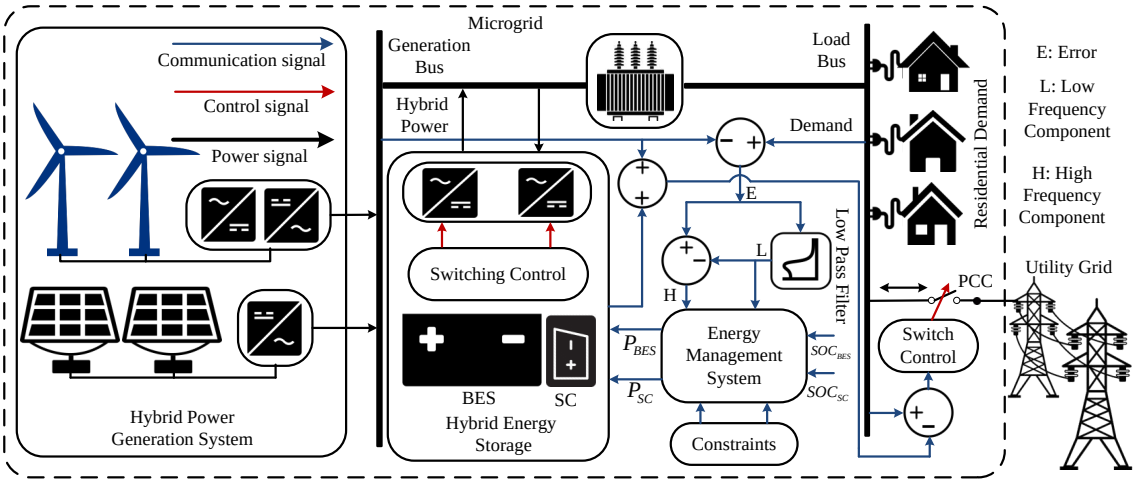

Figure 4.1: Block diagram of grid-connected MG system.

The remainder of the chapter is organized as follows. Section 2 presents the mathematical modeling of MG. The proposed methodology is demonstrated in Section 3. The information of the databases is provided in Section 4 and the Section 5 presents results and discussions.

4.2 Microgrid Modelling

The block diagram of the MG considered in this study is shown in Fig. 4.1, it utilizes PV-WT for hybrid power generation and BES-SC for hybrid energy storage. A hybrid RE system, employing two or more RE sources, mitigates the intermittent nature of RE resources to some extent and also improves the system efficiency. The PV and WT are coupled to generation bus through DC/AC and AC/AC converters respectively, and HESS is connected to AC bus via bidirectional DC/AC converter. The residential load is taped from the load bus via step down coupling transformers, and the utility grid (UG) is also connected to the load bus at point of common coupling (PCC) through a

controlled switch.

4.2.1 Wind Power Generation System

The mathematical model of wind power generation system presented in 3.3.1 is used.

4.2.2 Solar Photovoltaic Generation System

The mathematical model of solar photovoltaic generation system presented in 3.3.2 is used.

4.2.3 Battery Energy Storage System

A BES system consists of series and parallel strings of batteries. Several types of battery energy storage technologies are available having different chemistry, depth of discharge, number of cycles, etc. In this work, Sodium Sulphur (NaS) type battery energy storage is considered. NaS is one of the batteries used for commercial electrical energy storage in electric utility distribution grid support, wind power integration and high-value grid services. Its applications include load levelling, peak shaving and power quality as well as RE management and integration. A BES model, as given in [133], is calculated as given below

$$Charge : E_{BES}(t+\Delta t) = E_{BES}(t) + \Delta t P^{c}_{BES} \eta_c \tag{4.1}$$

$$Disharge : E_{BES}(t+\Delta t) = E_{BES}(t) - \Delta t \frac{P^{d}_{BES}}{\eta_d} \tag{4.2}$$

Charging/discharging constraints are

$$0 \leq P_{BES}^{c} \leq P_{BES}^{cmax} \tag{4.3}$$

$$0 \leq P_{BES}^{d} \leq P_{BES}^{dmax} \tag{4.4}$$

Stored energy bounds are

$$E_{BES}^{min} \leq E_{BES}(t) \leq E_{BES}^{max} \tag{4.5}$$

where E_{BES} is the energy stored in the battery, i.e., state-of-charge, P_{BES}^{c} and P_{BES}^{d} are charging and discharging powers respectively, and η_c is charging efficiency and η_d is discharging efficiency of the battery.

4.2.4 Supercapacitor

Energy stored in the SC at any instant is modeled as

$$E_{SC}(t+\Delta t) = E_{SC}(t) + \eta \Delta t P_{SC} - \xi E_{SC}(t) \tag{4.6}$$

subjected to the following constraints

$$E_{SC}^{min} \leq E_{SC}(t) \leq E_{SC}^{max} \tag{4.7}$$

$$0 \leq P_{SC}(t) \leq P_{SC}^{max} \tag{4.8}$$

where E_{SC} is the energy stored in SC, η is charging/discharging efficiency, ξ is self-discharge rate, and P_{SC} is the power supplied/drawn to/from the SC. During charging period P_{SC} is positive while it is negative during discharging period. The (4.7) represents the stored energy constraint whereas (4.8) represents the bounds for power supplied/drawn to/from the SC.

4.2.5 Utillity Grid

Utility grid serves two important objectives, (i) ensures load and generation always to be equal by supplying the demand whenever MG generation is lower than demand, and (ii) buys energy from the MG during surplus generation hours to make the system more economical. The power of UG at any instant of time can be modeled as

$$P_{grid}(t) = P_L(t) - \sum (P_{WT}(t), P_{PV}(t), P_{BES}(t), P_{SC}(t)) \tag{4.9}$$

where P_{grid} is the power supplied to/from the UG, P_L is load demand, P_{BES} is the power supplied by BES and P_{SC} is the power supplied by SC. During surplus generation hours P_{grid} is negative while positive during inadequate supply hours.

4.3 Proposed Methodology

The proposed methodology is further divided into five sub-sections. Section 4.3.1 presents methodology for sizing of RE sources, and HESS sizing strategy is discussed in detail in Section 4.3.2. Reliability and economic modeling is discussed in Section 4.3.3, while modeling of GHG emissions is presented in Section 4.3.4. Finally, the objective function formulation is given in Section 4.3.5.

4.3.1 Renewable Energy Sources Sizing

The BSA developed in Section 3.4.1 is applied to determine the sizes of RE sources.

4.3.2 Hybrid Energy Storage System Sizing

Power generated by any combination selected from the reduced search space is calculated using following equation

$$P_G^u(t) = N_{PV}^{min^u} P_{PV}(t) + N_{WT}^{min^u} P_{WT}(t) \qquad \forall t > 0 \tag{4.10}$$

subjected to following constraints

$$N_{PV}^{min^1} \leq N_{PV}^{min^u} \leq N_{PV}^{min^j_{max}}$$

$$N_{WT}^{min^1} \leq N_{WT}^{min^u} \leq N_{WT}^{min^j_{max}}$$

where P_G is the power generated by the MG and u is the case number. The difference between power generated and power demanded for case u at any instant of time is denoted by p^u_{gap} and calculated as follows

$$p^u_{gap}(t) = P_L(t) - P^u_G(t) \qquad \forall t > 0 \tag{4.11}$$

The p_{gap} is divided into two components, i.e., high frequency and low frequency components as shown in Fig. 4.1. The high frequency component is used for the sizing of SC and the low frequency component is used for the sizing of BES. The algorithm for dividing p_{gap} into high and low frequency components can be realized by low pass energy filter whose transfer function is given below

$$H(s) = \frac{K\omega_o^2}{s^2 + (\omega_o/Q) + \omega_o^2} \tag{4.12}$$

$$p^u_{gap} = p^u_{gap-H} + p^u_{gap-L} \tag{4.13}$$

where ω_o is cut-off frequency, p_{gap-H} is high frequency component, and p_{gap-L} is low frequency component. The maximum capacities of BES and SC that can be employed to store all of the excess energy are determined by using the algorithms given below. These algorithms represent the operation of BES and SC based upon which their maximum capacities, that can be installed, have been calculated.

$$P^u_{gap-H}(\hbar) = \begin{cases} P^u_{gap-H}(\hbar) & P^u_{gap-H}(\hbar) > 0 \\ 0 & otherwise \end{cases} \qquad \forall \hbar \tag{4.14}$$

where

$$P^u_{gap-H}(\hbar) = \sum_{t=1}^{\hbar} p^u_{gap-H}(t) \tag{4.15}$$

The maximum SC size is calculated as

$$C^u_{max} = max(P^u_{gap-H}) \tag{4.16}$$

Similarly, for BES we have

$$P^u_{gap-L}(\hbar) = \begin{cases} P^u_{gap-L}(\hbar) & P^u_{gap-L}(\hbar) > 0 \\ 0 & otherwise \end{cases} \qquad \forall \hbar \tag{4.17}$$

where

$$P^u_{gap-L}(\hbar) = \sum_{t=1}^{\hbar} p^u_{gap-L}(t) \tag{4.18}$$

The maximum capacity of BES is calculated as

$$B^u_{max} = max(P^u_{gap-L}) \tag{4.19}$$

where B_{max} and C_{max} are the maximum capacities of BES and SC. Required capacities of BES and SC would be less than or equal to B_{max} and C_{max} which are calculated as

$$B^u_{cap} = \begin{cases} B^u_{max} & x = 1 \\ CBS^u & x = 0 \end{cases} \tag{4.20}$$

where B_{cap} is the required energy capacity of battery. The B_{cap} is equal to B_{max} if the battery discharges completely after the full charging period and this condition is indicated by $x = 1$. While the B_{cap} is equal to corrected battery size CBS if the battery does not discharge fully after its full charging period, this condition is indicated by $x = 0$. The condition $x = 0$ implies that the battery is over-sized. An iterative region elimination algorithm is used to calculate CBS which is defined by following equations:

$$CBS^u(w) = \frac{S^u_{min}(w) + S^u_{max}(w)}{2} \tag{4.21}$$

where

$$S^u_{min}(w+1) = \begin{cases} S^u_{min}(w) & x = 1 \\ CBS(w) & x = 0 \end{cases} \tag{4.22}$$

and

$$S^u_{max}(w+1) = \begin{cases} S^u_{max}(w) & x = 0 \\ CBS(w) & x = 1 \end{cases} \tag{4.23}$$

$$STEP^u_a = S^u_{max}(w) - S^u_{min}(w) \tag{4.24}$$

where S_{min} and S_{max} are the minimum and maximum boundaries of solution, $STEP_a$ is the difference between the minimum and maximum boundaries, and w is the iteration

number. Initially, S_{min} and S_{max} are set equal to 0 and B_{max} respectively. Both of them get updated in an iterative fashion until $STEP_a$ becomes less than or equal to the allowable tolerance e. Similar calculations that are given in (4.20)-(4.24) can be repeated (just with a little modification in the constraints while calculating x) to find the required size of SC (C_{cap}). The B_{cap} and C_{cap} are the required sizes but both are not optimal. If they are installed, the system will be reliable but not efficient and economical.

An important parameter that needs to be checked is utilization factor; higher value of utilization factor reduces the idle time and ensures the maximum benefit from BES and SC. Therefore, utilization factor is used to determine the optimal capacities of BES and SC. In order to calculate the utilization factor, battery decision variable BDV is computed as

$$BDV^u = \frac{\sum B^u_{chg-dcg}(t)}{n} \qquad \forall t > 0 \tag{4.25}$$

where

$$B^u_{chg-dcg}(t) = \begin{cases} 1 & |P^u_{gap}(t) - P^u_{gap}(t-\Delta t)| \geq \lambda P^u_{BES_{max}} \\ 0 & else \end{cases} \quad \forall t > 0 \tag{4.26}$$

where $B_{chg-dcg}$ is the battery charging and discharging factor which is equal to one when the charging or discharging power is greater than or equal to $\lambda P_{BES_{max}}$, where λ is a constant which can take a value btween 0 and 1. Hence, optimal size of BES is calculated as

$$B^u_{opt} = \begin{cases} B^u_{cap} & BDV^u \geq B_{lim} \\ BCS^u & else \end{cases} \tag{4.27}$$

where B_{opt} is the optimal capacity of BES and B_{lim} is the minimum battery utilization limit. The B_{opt} equals to B_{cap} if BDV becomes greater than or equal to B_{lim} otherwise B_{opt} equals to battery corrected size BCS. The BCS is calculated using a region elimination iterative search algorithm as following

$$BCS^u(w) = \frac{OCF^u_{min}(w) + OCF^u_{max}(w)}{2} \tag{4.28}$$

where

$$OCF^u_{min}(w+1) = \begin{cases} OCF^u_{min}(w) & BDV^u \geq BU_{lim} \\ BCS^u(w) & else \end{cases} \tag{4.29}$$

and

$$OCF^u_{max}(w+1) = \begin{cases} BCS(w) & BDV^u \geq BU_{lim} \\ OCF^u_{max}(w) & else \end{cases} \tag{4.30}$$

$$STEP^u_b = OCF^u_{max}(w) - OCF^u_{min}(w) \tag{4.31}$$

where OCF_{min} and OCF_{max} are the minimum and maximum boundaries of solution respectively and $STEP_b$ is the error between minimum and maximum boundaries. Initially, OCF_{min} and OCF_{max} are set equal to 0 and B^u_{cap} and both of them get updated in the iterative algorithm until $STEP_b$ reaches below the allowable tolerance e. Similar

calculations that are given in (4.27)-(4.31) are repeated (just with a little modification in the constraints while calculating BDV) to find optimal size of SC (C_{opt}). This process of calculation of B_{opt} and C_{opt} is repeated for all combinations of N_{PV} and N_{WT} that are selected for the $\mathbf{RS_{space}}$.

4.3.3 Reliability and Economic Modeling

Reliability and cost are two important parameters that can be used to analyze the performance of a system. A power system having lower cost, higher reliability (i.e., energy served), and lower GHG emissions can be considered to have better performance. In this study, the optimal solution is determined on the basis of cost, reliability, and GHG emissions.

The total generation of MG after finding the optimal size of the HESS, i.e., B_{opt} and C_{opt} for u^{th} combination of PV and WT is calculated as following

$$P^{u}_{GT}(t) = N^{min^{u}}_{PV} P_{PV}(t) + N^{min^{u}}_{WT} P_{WT}(t) + P^{u}_{Bat}(t) + P^{u}_{Cap}(t) \tag{4.32}$$

where P_{GT} is the total power generated by MG, P_{Bat} is the power supplied by battery and P_{Cap} is the power supplied by SC. Energy served is the summation of demand that is served by the MG over a period of its operation.

$$E^{u}_{S} = \sum_{t=1}^{n} D^{u}(t) \tag{4.33}$$

where

$$D^u(t) = \begin{cases} P_L(t) & P^u_{GT}(t) \geq P_L(t) \\ P^u_{GT}(t) & otherwise \end{cases} \qquad \forall t > 0 \tag{4.34}$$

where E_S is energy served, P_L is the load power demand, and P_{GT} is total generation of the MG. Energy not served E_{NS} is the summation of demand that is not supplied by the MG during its operation.

$$E^u_{NS} = \sum_{t=1}^{n} G^u(t) \tag{4.35}$$

where

$$G^u(t) = \begin{cases} P_L(t) - P^u_{GT}(t) & P_L(t) > P^u_{GT}(t) \\ 0 & otherwise \end{cases} \qquad \forall t > 0 \tag{4.36}$$

Net discounted energy served is calculated as

$$NDE^u_S = E^u_S PWF \tag{4.37}$$

where

$$PWF = \left[\frac{(1+d)^l - 1}{d\,(1+d)^l} \right] \tag{4.38}$$

where PWF is the present worth factor, l is the year of operation, and NDE^u_S is the net discounted energy served by the MG.

As discussed earlier, cost is also an important parameter that can be used to assess the performance of a system. In this work initial investment cost, fixed and variable operation and maintenance costs, storage replacement cost, and cost of energy exchanged

between MG and UG are considered. The following relation is used to determine the investment cost associated with RE sources

$$C^{u}_{inv-sc} = \sum_{k=1}^{N} C^{k}_{c,sr} P^{k,u}_{sr} \tag{4.39}$$

where C_{inv-sc} is the total investment cost of RE sources, $C^{k}_{c,sr}$ is the capital cost of k^{th} source in \$/MW, P^{k}_{sr} is the installed capacity of k^{th} source in MW, and N is the total number of RE sources. The investment cost of storage system is calculated as follows

$$C^{u}_{inv-stg} = \sum_{k=1}^{M} \left(C^{k}_{c,stg} E^{k,u}_{stg} + C^{k}_{c,pcs} P^{k,u}_{stg} \right) \tag{4.40}$$

where $C^{k}_{c,stg}$ is the capital cost of k^{th} storage unit in \$/MWh, E^{k}_{stg} is the energy capacity of k^{th} storage unit in MWh, $C^{k}_{c,pcs}$ is the cost of power conditioning system required for the storage in \$/MW, P^{k}_{stg} is the power capacity of k^{th} storage unit in MW, and M is the total number of storage units. The replacement cost of storage is modeled as following

$$C^{k,u}_{rep-stg} = \sum \frac{C^{k}_{c,stg} E^{k,u}_{stg}}{(1+d)^{s}} \qquad s = p, 2p, 3p, ...l - p \tag{4.41}$$

where d is the discount rate and p is the life of the storage in years. The operation and maintenance costs of the MG consist of fixed and variable operation and maintenance costs are calculated as follows

$$C^{u}_{om} = C^{u}_{om,f} + C^{u}_{om,v} \tag{4.42}$$

where

$$C^{u}_{om,f} = \sum_{t=1}^{n} \sum_{k=1}^{M+N} T^{k}(t) J^{k}_{om,f} P^{k}_{r} \tag{4.43}$$

and

$$C^{u}_{om,v} = \sum_{t=1}^{n} \sum_{k=1}^{M+N} J^{k}_{om,v} P^{k}(t) \tag{4.44}$$

where $C_{om,f}$ is the fixed operation and maintenance cost, T^{k} is the time of operation of k^{th} element, $J^{k}_{om,f}$ is the operation and maintenance cost factor in \$/MW-yr, and P^{k}_{r} is the rated power capacity of k^{th} element in MW. The variable operation and maintenance cost is referred by $C_{om,v}$, $J^{k}_{om,v}$ is the variable operation and maintenance cost factor in \$/MW, and $P^{k}(t)$ is the output power of k^{th} element at time t in MW. Net present value of C_{om} is calculated as

$$NPVC^{u}_{om} = C^{u}_{om} PWF \tag{4.45}$$

where $NPVC_{om}$ is the present worth of C_{om}.

During surplus generation hours, the MG sells energy to UG. Total cost and net present worth of the energy supplied by MG to UG is calculated as follows

$$C^{u}_{MG-U} = \sum_{t=1}^{n} C_{exchg}(t) P^{u}_{MG-U}(t) \tag{4.46}$$

$$NPVC^{u}_{MG-U} = C^{u}_{MG-U} PWF \tag{4.47}$$

where C_{MG-U} is the total cost of the energy sold by MG to UG, $C_{exchg}(t)$ is the cost

Table 4.1: Greenhouse Gases Emission Data

Greenhouse gases	CO_2	CO	SO_2	NOx
Emissions kg/MWh	1000.7	1.55	9.993	6.46
Correction Cost \$/kg	0.0037	0.16	0.97	1.29

at time t, $P_{MG-U}(t)$ is the power supplied by MG to UG at time t, and $NPVC_{MG-U}$ is the present worth of C_{MG-U}. In the event when MG generation is insufficient to meet the demand, the MG buys power from UG. Total cost and net present worth of energy supplied by the utility to MG is calculated using following equations

$$C^{u}_{U-MG} = \sum_{t=1}^{n} C_{exchg}(t)\, P^{u}_{U-MG}(t) \tag{4.48}$$

$$NPVC^{u}_{U-MG} = C^{u}_{U-MG} PWF \tag{4.49}$$

where C_{U-MG} is the total cost of energy supplied by UG to MG, $C_{exchg}(t)$ is the cost at time t, $P_{U-MG}(t)$ is the power supplied by UG to MG at time t, and $NPVC_{U-MG}$ is the present worth of C_{U-MG}.

4.3.4 Modeling of GHG Emissions

When electric power is generated by burning fossil fuels, it results in GHG emissions in the environment. There is a correction cost which is needed to mitigate the damage caused by these emissions as shown in Table 4.1. This correction cost would be a saving if the electric power is generated by utilizing RE sources instead of fossil fuels. This

saving is named as emission reduction benefit cost (ERBC), and modeled as

$$C^u_{ERB} = \sum_{k=1}^{4} \sum_{t=1}^{n} P^u_{GT}(t) E^k E^k_{cc} \tag{4.50}$$

where C_{ERB} is the total ERBC, $P_{GT}(t)$ is the power output of MG at time t, E^k is the emission of k^{th} type of GHG, and E^k_{cc} is the cost required to correct the damage caused by k^{th} type of GHG. The net present value of total ERBC is calculated using following equation as

$$NPVC^u_{ERB} = C^u_{ERB} PWF \tag{4.51}$$

where $NPVC_{ERB}$ is the present worth of ERBC.

4.3.5 Cost Function Formulation

The objective is to find an optimal combination of PV, WT, BES, and SC that must result in lower cost, higher reliability, and lower GHG emissions. Cost function of the optimization problem is formulated as following

$$obj : F^u = \sqrt{\left(f^u_1(\boldsymbol{X^u_1}, \boldsymbol{X^u_2}) - f^u_2(\boldsymbol{X^u_1}, \boldsymbol{X^u_2})\right)^2} \rightarrow \min \tag{4.52}$$

$$s.t. \begin{cases} \boldsymbol{g}_\ell(\boldsymbol{X^u_1}, \boldsymbol{X^u_2}) = 0 \quad \ell = 1,2,,...,m \\ \boldsymbol{h}_\iota(\boldsymbol{X^u_1}, \boldsymbol{X^u_2}) \leq 0 \quad \iota = 1,2,,...,q \end{cases} \tag{4.53}$$

where

$$\boldsymbol{X_1^u} = \left[N_{PV}^{min^u},\, N_{WT}^{min^u},\, P_{Cap}^u,\, P_{Bat}^u\right] \tag{4.54}$$

and

$$\boldsymbol{X_2^u} = \left[E_{Cap}^u,\, E_{Bat}^u,\, \omega_o^u\right] \tag{4.55}$$

The first term in the objective function is cost per unit of the MG. It is important to note that the initial investment cost of sources (4.39), initial investment cost of storage (4.40), operation and maintenance cost (4.45), replacement cost (4.41), cost of energy supplied by UG to MG (4.48), and energy served (4.37) are incorporated in the cost per unit of MG. Second term of the objective function represents the GHG emissions that are translated in terms of cost using ERBC concept as discussed in Section 4.3.4. The equality constraints are referred by $\boldsymbol{g}$ and in-equality constraints are referred by $\boldsymbol{h}$. All system constraints are summarized as:

The Pimary System Constraint (Generation = Demand):

$$P_{GT}^u + P_{U-MG}^u - P_L - P_{MG-U}^u = 0 \tag{4.56}$$

The hybrid power generation constraints:

$$N_{PV}^{min^1} \leq N_{PV}^{min^u} \leq N_{PV}^{min^j} \tag{4.57}$$

$$N_{WT}^{min^1} \leq N_{WT}^{min^u} \leq N_{WT}^{min^j} \tag{4.58}$$

BES Constraints:

$$0 \leq P_{BES}^{c} \leq P_{BES}^{cmax} \tag{4.59}$$

$$0 \leq P_{BES}^{d} \leq P_{BES}^{dmax} \tag{4.60}$$

$$E_{BES}^{min} \leq E_{BES}(t) \leq E_{BES}^{max} \tag{4.61}$$

SC Constraints:

$$E_{SC}^{min} \leq E_{SC}(t) \leq E_{SC}^{max} \tag{4.62}$$

$$0 \leq P_{SC}(t) \leq P_{SC}^{max} \tag{4.63}$$

Switching Frequency Constraint:

$$0 \leq \omega_{o}^{u} \leq 1 \tag{4.64}$$

A solution space is generated which contains the values of cost function that correspond to all j_{max} combinations of PV, WT, BES, and SC. Solution space is given as follows

$$\boldsymbol{SS} = \left[F^{1}\ F^{2} \ldots F^{j_{max}}\right]_{1 \times j_{max}} \tag{4.65}$$

where $\boldsymbol{SS}$ is the solution space and F is value of the objective function. There are j_{max} possible solutions each corresponding to one combination. The best solution from the $\boldsymbol{SS}$ is selected based upon minimum value of the cost function by using a minima search algorithm. The pseudocode of the optimal sizing is given in Algorithm I.

Algorithm I Optimal Capacity Sizing

Start

Initialization: $i \leftarrow 1$, $j \leftarrow 1$, $t \leftarrow 1$, $u \leftarrow 1$, $e \leftarrow 0.1$

- **Data Generation**

Read: c, σ, I, α, β, γ, ρ, $Load$

Calculate: P_{PV}, P_{WT}, P_L, N_{PV}^{min}, N_{WT}^{min}, N_{PV}^{max}, N_{WT}^{max}, P_G (3.5), (3.4), (3.14)-(3.17)

Save: P_{PV}, P_{WT}, P_L, N_{PV}^{min}, N_{WT}^{min}, N_{PV}^{max}, N_{WT}^{max}, P_G

- **Search Space Formation**

While $i \leq i_{max}$ **Do**

  While $j \leq j_{max}$ **Do**

    Calculate: $\Delta P^{(i,j)}$, $\boldsymbol{\Delta P}$ (3.18), (3.19)

    Save: $\boldsymbol{\Delta P}$, $\mathbf{N_{PV}}$, $\mathbf{N_{WT}}$

    Calculate: $\mathbf{S_{space}}$ (3.23)

    $j \leftarrow j+1$

  End While

  $i \leftarrow i+1$

End While

- **Reduced Search Space Formation**

While $j \leq j_{max}+1$ **Do**

While $i \leq i_{max}+1$ **Do**

Calculate: ΔP^{j}_{min}, $N^{j}_{PV_{min}}$, $N^{j}_{WT_{min}}$ (3.25)

$i \leftarrow i+1$

End While

Calculate: $\mathbf{\Delta P_{min}}$, $\mathbf{N_{PV_{min}}}$, $\mathbf{N_{WT_{min}}}$

$j \leftarrow j+1$

End While

Calculate: $\mathbf{RS_{space}}$ (3.28)

- **HESS Sizing**

While $u \leq j_{max}$ **Do**

Call PSO

Calculate: P^{u}_{G}, p^{u}_{gap}, ω_o, P^{u}_{gap-H}, P^{u}_{gap-L} (4.10), (4.11), (4.12)

- **Required size of BESS and SC**

Calculate: B^{u}_{max}, x, C^{u}_{max}, (4.19), (4.16)

Call Region reduction iterative search algorithm (4.20)-(4.24)

- **Optimal size of BESS and SC**

Calculate: BDV^{u}, $B^{u}_{chg-dcg}$ (4.25), (4.26)

Call Region reduction iterative search algorithm (4.27)-(4.31)

Calculate: P^{u}_{GT}, E^{u}_{S}, E^{u}_{NS}, F^{u}, (4.32) (4.33), (4.35), (4.52)

$u \leftarrow u + 1$

End While

- **Determination of the optimal solution**

  Generate: $\boldsymbol{SS}$ (4.65)

  Call Minima search algorithm

  Optimal solution

End

4.4 Databases

As mentioned earlier, the proposed methodology is tested using real-world data of wind speed, solar irradiation and power demand from Dammam city in Saudi Arabia. The Dammam city lies in the eastern province of Kingdom of Saudi Arabia and its coordinates are 26.3927N, 49.9777E. The wind speed is calculated using the shape and scale parameters of Weibull distribution. The shape and scale parameters were determined using well maintained meteorological data of wind of 20 years [134]. Monthly shape and scale parameters are given in Table 3.1. The normalized daily average residential power demand of the calendar year 2015 is presented in Fig. 4.2, which depicts that the daily peak occurs around 8 pm while minimum demand appears around 7 am. The normalized daily average solar irradiation is shown in Fig. 4.3 showing irradiation peak at around 1pm. Whereas the normalized daily average wind speed is shown in Fig. 4.4. It can be observed that wind speed is variable and fluctuates throughout the day.

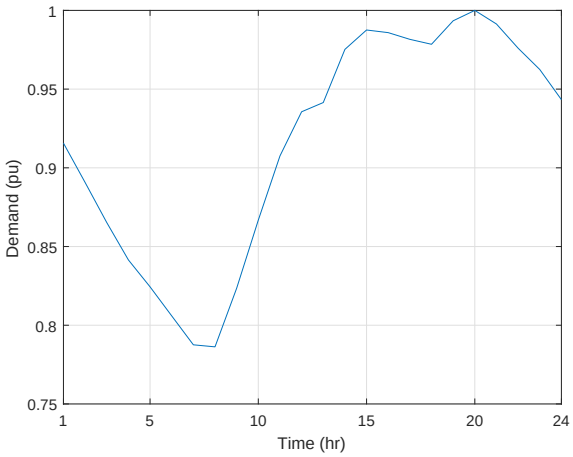

Figure 4.2: Normalized average daily power demand of Dammam of calendar year 2015.

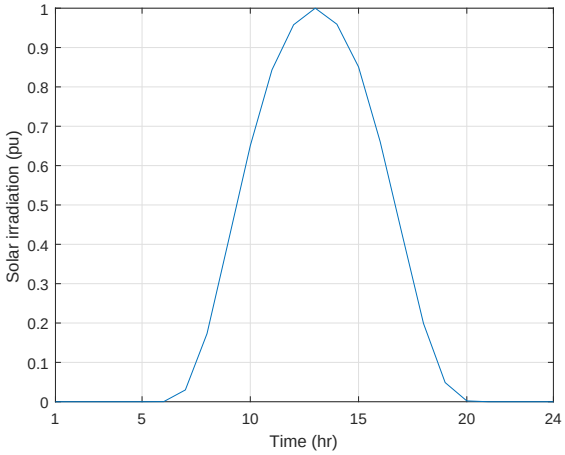

Figure 4.3: Normalized daily average solar irradiation.

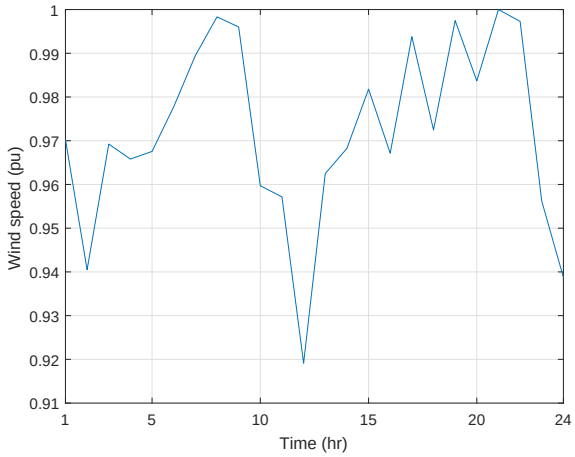

Figure 4.4: Normalized daily average wind speed.

4.5 Simulation Results and Discussions

The first step in our proposed methodology is to find combinations of PV and WT for the reduced search space given in (3.28). The determination of the combinations is based upon minimization of the cumulative error between load and generation, defined in (3.19), so that renewable power generation should have better load following. The algorithm given in Section 3.4.1 has selected 800 combinations of PV and WT. As mentioned earlier, RE sources perform effectively when operated with properly sized and suitable type of energy storage. The optimal size of ESS is characterized by both energy storing capacity and maximum power rating. Second step of the strategy is to determine the energy (MWh) and power (MW) capacities of BES system and SC storage. Finally, the optimal combination of PV, WT, BES, and SC is determined based upon three important parameters, i.e., cost, reliability, and GHG emissions. The solution space, as given in (4.65), is formulated and shown in Fig. 4.5. It is important to note that for each index of solution space there is a combination of PV, WT, BES, and

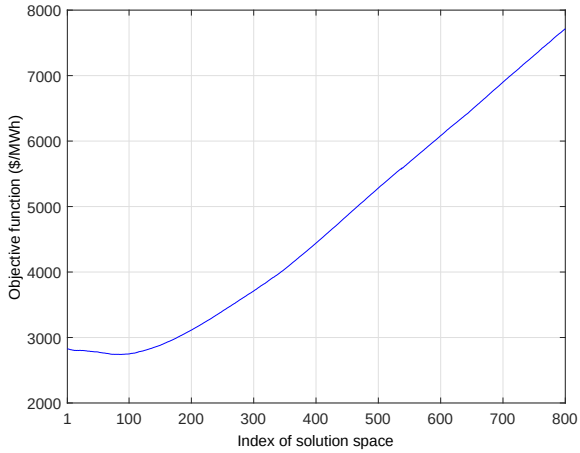

Figure 4.5: Variation in the cost function w.r.t index of the solution space.

SC, and optimal combination corresponds to the index with minimum value of objective function. A smaller value of the objective function implies that the energy supplied by the MG is larger, cost per unit of the MG is smaller, GHG emissions are lesser, and emission reduction benefit cost (as defined in (4.50)) is higher. In the presented case study, the minimum value of cost function appears corresponding to index number 88 which can be seen in Fig. 4.5.

The optimal capacities of PV, WT, BES, and SC are given in Table 4.2. The overall cost per unit is USD 0.1552. It is important to note that the cost per unit is the function of many parameters, for example a location with higher correlation between the solar irradiation curve, wind speed curve and load curve would result in further reduction in

Table 4.2: Optimal Capacities Combination

Source Type	Solar (MW)	Wind (MW)	BES (MWh,MW)	SC (MWh,MW)
Capacity	87	88	48 9.6	4.4 52

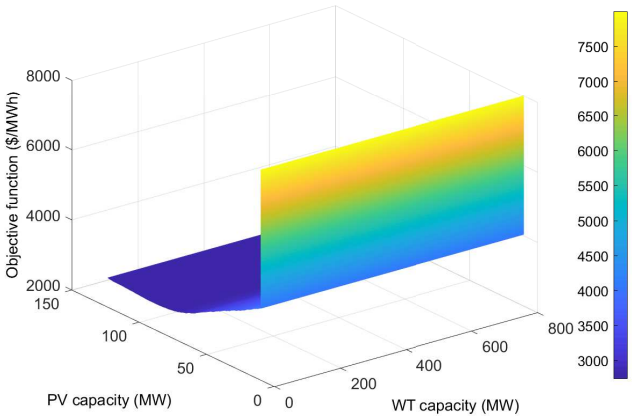

Figure 4.6: Cost function vs different combinations of PV and WT.

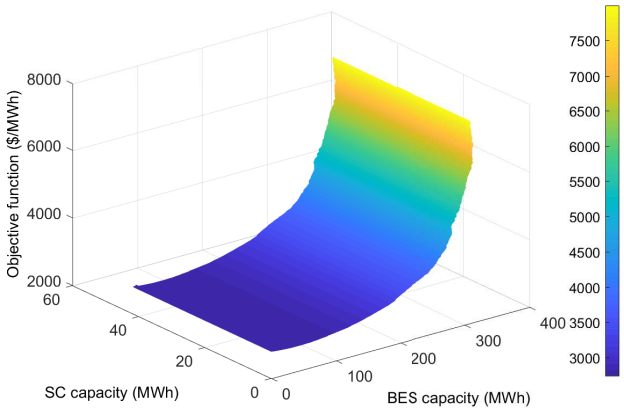

Figure 4.7: Cost function vs different combinations of SC and BES.

cost, and our optimized solution will then be more effective and justified.

In order to get more comprehensible insight in variations of the cost function with RE sources and HESS capacities, the cost function is plotted against the combinations of PV and WT, and SC and BES, that corresponds to each index of solution space shown in Fig. 4.6 and Fig. 4.7 respectively.

Initially, the installed capacities of both RE sources and HESS are small while values of the cost function are higher because GHG emissions are higher, energy served

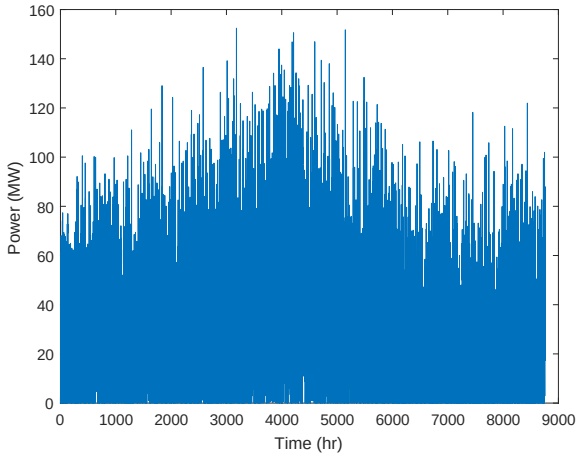

Figure 4.8: Hybrid power generation.

by the MG is lesser, and ERBC is also small. With the increase in the installed capacities, corresponding values of the cost function decrease because energy supplied by the MG increases which results in lower GHG emissions and increased ERBC. Although, per unit cost also increases with the increase in the installed capacities but its impact on the objective function is non-dominant for moderate capacities. However, for very large capacities, values of the objective function are high because the impact of cost of RE sources and HESS on objective function becomes dominant. Although, for very large capacities energy supplied by the MG is higher, GHG emissions are lesser and ERBC is also higher but their impact on the cost function is less dominant as compared to the cost of RE sources and HESS. The cost of BES and SC is very high so for larger capacities they have large impact on overall cost of the MG.

The hybrid power generated by optimal PV-WT system and the load power demand are shown in Fig. 4.8 and Fig. 4.9 respectively. While the error/gap between the generation and demand is plotted in Fig. 4.10. This error is required to be supplied to/by energy storage system, which is HESS in our case. The error signal is supplied

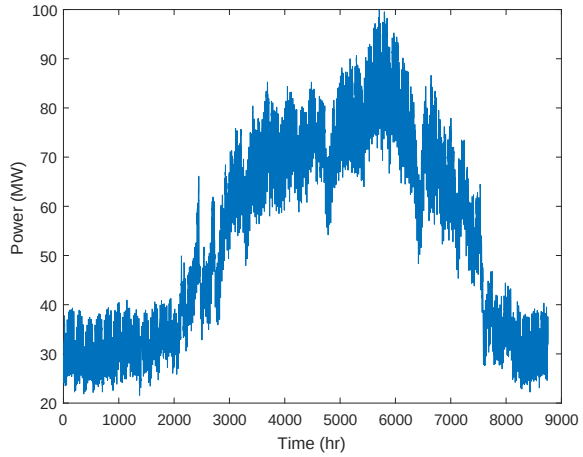

Figure 4.9: Load power demand.

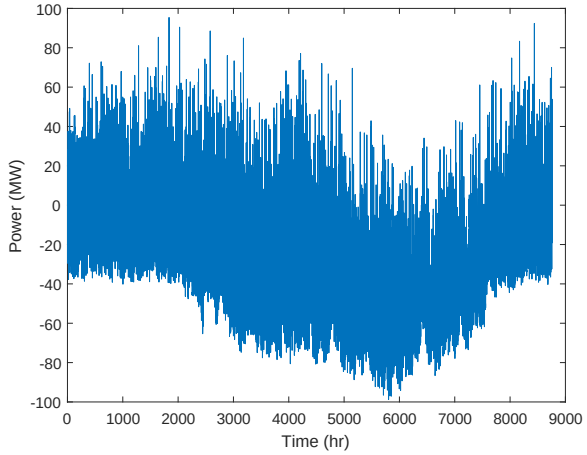

Figure 4.10: Difference in generation and demand.

to/by BES and/or SC depending upon its magnitude and frequency. A histogram of the error signal is presented in Fig. 4.11 which shows that most of the times the magnitude of error is more than the rated power capacity of BES system. However, most of the times the error signals can be supplied by utilizing the HESS system.

A comparison based upon cost per unit of the MG, GHG emissions, energy served by the MG, and ERBC, between four different possible solutions selected from the solution space, is tabulated in Table 4.3. Cost per kWh of the MG is minimum for Case

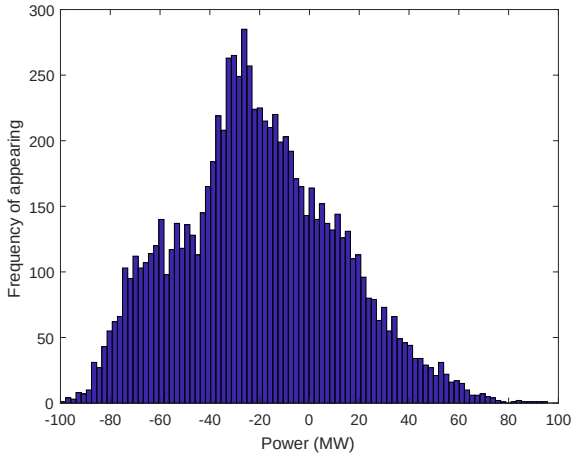

Figure 4.11: Histogram of gap between generation and demand.

number 2 and maximum for Case number 4, since installed capacities in this case are very high. The GHG emissions are minimum for Case number 4 while maximum for Case number 1, and moderate for Case number 2 and 3. Energy served is highest for Case number 4 whilst lowest for Case number 1 and moderate for Case number 2. As the optimal solution is determined based upon the cost, reliability, i.e., energy served, and GHG emissions, Table 4.3 clearly shows that Case number 2 is optimal.

As mentioned earlier that the output of RE sources is variable, so it may happen during the operation of the MG that output of the RE sources and storage system be-

Table 4.3: Comparison Between Different Possible Solutions

Case No.	Index No.	PV (MW)	WT (MW)	BES (MWh)	SC (MWh)	MG Generation Cost ($/kWh)	GHG Emissions (kt)	Energy Served (GWh)	ERBC (M$)
1	60	100	60	28	3.4	0.28	245	237	5.21
2	**88**	**87**	**88**	**48**	**4.4**	**0.27**	**213**	**269**	**5.90**
3	200	54	200	166	10	0.315	117	362	7.97
4	800	10	800	308	42	0.801	15	463	10.18

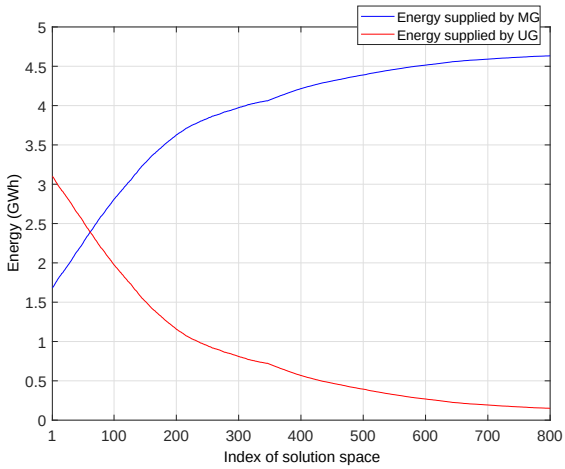

Figure 4.12: Energy share of MG and UG.

comes inadequate to supply the required load demand, during such events, the MG buys power from UG in order to meet the demand. Total energy share supplied by the MG and the UG to fulfill the required load demand is shown in Fig. 4.12. It can be observed that with the increase in indices the energy supplied by the MG increases while energy supplied by UG decreases. In the beginning, energy supplied by MG increases and energy supplied by utility decreases rapidly and finally both saturates.

The variation in the GHG emissions and ERBC with the indices of solution space are shown in the Figs. 4.13 and 4.14 respectively. It can be depicted that GHG emissions decrease while ERBC increases with the increase in the index (as overall installed capacities of RE sources and HESS increase with the increase in the index). It can be observed from Fig. 4.13 that the GHG emissions for the optimal solution are almost 55% less as compared to the conventional generation.

The operation of the MG over a period of one year with the optimal parameters is shown in Fig. 4.15. It can be observed that the system supplies the required demand effectively. As the system under consideration is grid-connected that is why the genera-

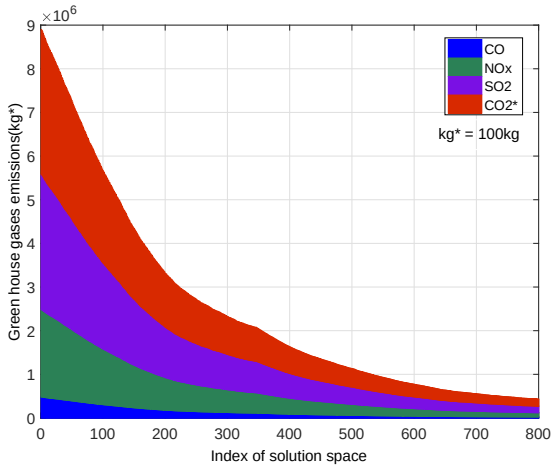

Figure 4.13: Variation in GHG emissions.

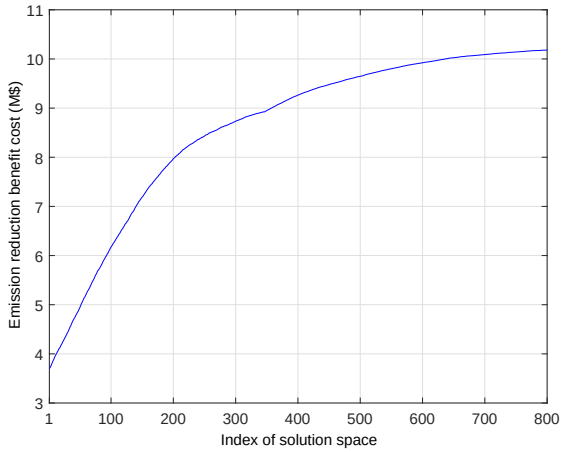

Figure 4.14: Emission reduction benefit cost.

tion is always equal to the required load power demand which makes the system highly reliable.

A comparison between the following three case studies is presented in Table 4.4.

- CASE-I: PV/WT/BES/SC based grid-connected MG.
- CASE-II: PV/WT/BES based grid-connected MG.
- CASE-III: A MG employing conventional generation.

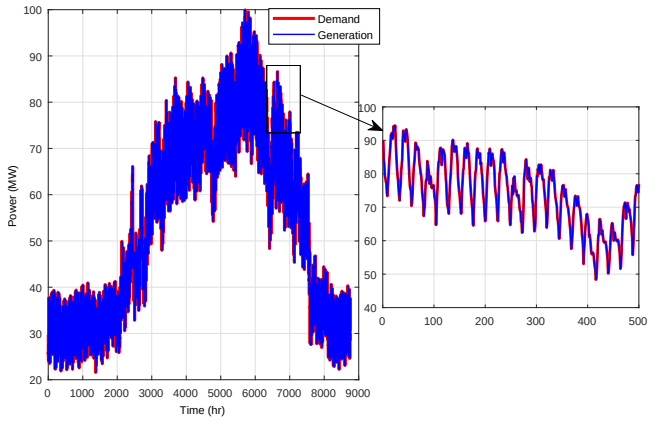

Figure 4.15: Actual demand vs supplied power with optimal system parameters.

Table 4.4: Comparison of Different Case Studies

Index		CASE-I	CASE-II	CASE-III
WT (MW)		88	88	0.0
PV (MW)		87	87	0.0
BES (MWh)		48	49	0.0
SC (MWh)		4.4	0.0	0.0
Energy (GWh)	MG	269	266	0.0
	Utility	209	212	478
Emissions (T)	CO	357	362	817
	CO_2	230544	233854	527274
	NOx	1488	1510	3404
	SO_2	2302	2335	5265
Cost ($/MWh)		155.2	155.4	100
ERBC (M$)		5.9	5.8	0.0

The cost per unit of the CASE-I is 0.13% less than that of CASE-II. This can result in savings of about USD 1M per year as compared to CASE-II. So, by employing the HESS instead of BES system, cost per unit decreases which results in considerable savings. This decrease in the cost is due to the fact that the SC prolongs the lifespan of BES system. The clean energy (energy from MG) supplied by the CASE-I is more than that of CASE-II. Similarly, the emissions are minimum for CASE-I and maximum for CASE-III. The emissions for CASE-I are approximately 55% less than that of CASE-III. These less GHG emissions also result in considerable savings in terms of ERBC and it can be seen from the Table 4.4 that the ERBC is maximum for CASE-I. So, the HESS is not only economical but also more reliable and cleaner as compared to BES.

CHAPTER 5

AN IMPROVED OPTIMAL SIZING METHODOLOGY FOR THE FUTURE SMALL AUTONOMOUS RESIDENTIAL SMART POWER SYSTEMS

5.1 Introduction

Accelerated development of eco-friendly technologies such as renewable energy (RE), smart grids, and electric transportation will shape the future of electric power generation and supply. The power consumption characteristics of modern power systems are designed to be more flexible and easily controllable, which will also effect the sizing of power generation system. This chapter presents a methodology for the capacity optimization of a typical residential standalone microgrid (MG) employing RE sources, i.e., solar photovoltaic (PV) panels, wind turbines (WTs), battery energy storage (BES) system, and diesel generators (DGs). The community load comprised of typical residential load demand and electric vehicle (EV) charging load is considered. The mathematical models of PV, WT, BES system, diesel generation system, and EV load are formulated to develop the capacity optimization methodology and it involves various realistic constraints associated with the RE sources, BES system, diesel generation system, and EV load. The labyrinthine optimization problem is formulated and solved innovatively to (i) minimize the cost, (ii) reduce greenhouse gases (GHG) emissions, and (iii) curtail dump energy. All three objectives have special significance in designing a standalone MG, for example, cost is related to the economics, GHG emissions deal with global warming, and dump energy is related to the stability and economics of the system. The optimization problem is solved for different possible combinations of PV, WT, BES, and DG to determine the best possible combination to serve the load effectively and economically. Using the idea of controllable loads the impact of load shifting on the sizes of distributed generators and BES system, per-unit cost, and GHG emissions is

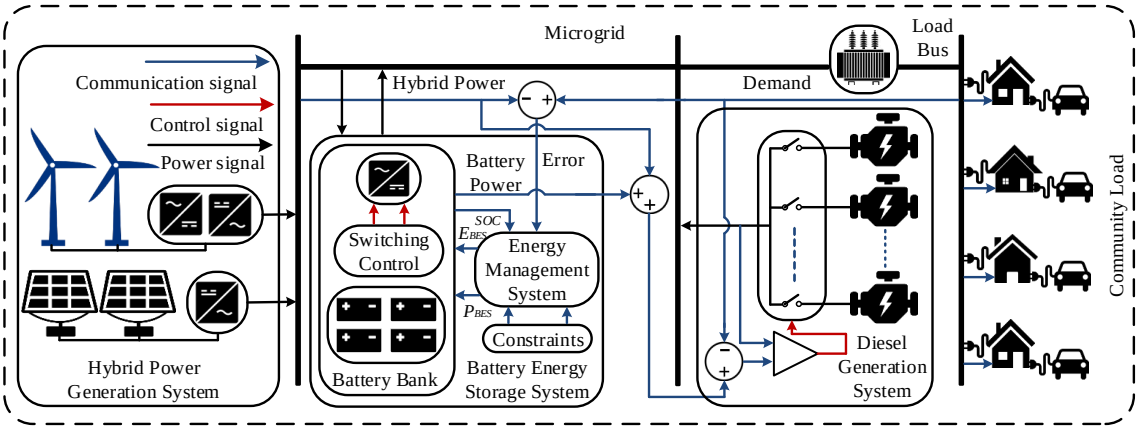

Figure 5.1: A stand-alone MG system.

also investigated.

The remainder of the chapter is organized as follows. Section 2 presents the detailed modeling of MG. The proposed methodology is demonstrated in Section 3. The information of the databases is provided in Section 4 and results and discussions are presented in Section 5.

5.2 Microgrid Modeling

A stand-alone MG system employing PV panels, WTs, BES system, and DGs to supply a typical residential demand is considered in this study, shown in Fig. 5.1. The MG system has four major parts: hybrid power generation system (HPGS), battery energy storage system, diesel generation system, and community load demand.

5.2.1 Hybrid Power Generation System Modeling

The HPGS consists of RE sources, i.e., PV and WT. The PV system is connected to the ac bus via DC-to-AC converter while WT system is connected to the ac bus via AC-to-

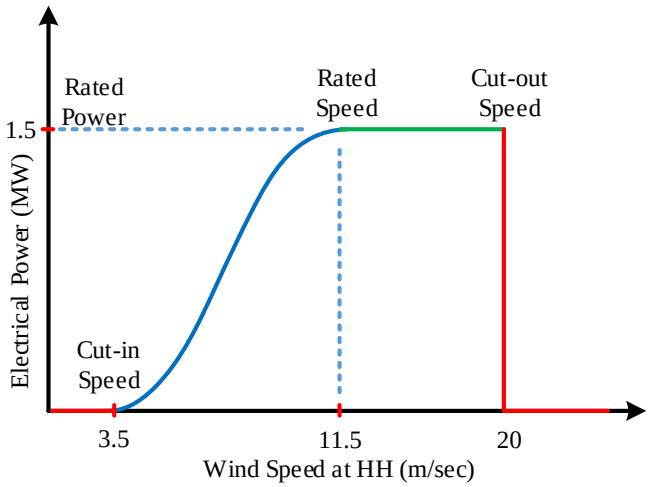

Figure 5.2: Power curve of GE 1.5xle WT.

AC converter. The power output of a solar PV system depends on solar irradiation, area and efficiency of the PV array, angle of incidence, and atmospheric temperature. In this study, it is assumed that a maximum power point tracker (MPPT) is installed to harvest the maximal of available power. The power generated by single PV panel at any instant of time can be calculated using the following equation [131]

$$P_{pv}(t) = \eta_{pv} A_{pv} I(t) (1 - 0.005 (T_o(t) - 25)) \tag{5.1}$$

where P_{pv} is the power output of PV system in W, η_{pv} and A_{pv} are the efficiency and area in m^2 of PV panel, T_o is the atmospheric temperature in ^oC, and I is the solar irradiation in W/m^2. The power output of a WT depends upon the wind speed and hub height (HH). In this study, the characteristics GE 1.5xle turbine are used to calculate the wind power output [135]. GE 1.5xle is one of the most commonly used WTs in the industry. The power curve of GE 1.5xle turbine is shown in Fig.5.2. The power output of the WT is modeled as given below

$$P_{wt}(v) = \begin{cases} 0 & v < v_{ci} \\ \psi(v) & v_{ci} \leq v < v_r \\ P_{wt}^r & v_r \leq v < v_{co} \\ 0 & v \geq v_{co} \end{cases} \tag{5.2}$$

where P_{wt} is the power output of WT in W, v is the wind speed in m/sec, P_{wt}^r is the rated power of WT in W, and v_{ci}, v_{co}, and v_r are the cut-in, cut-out, and rated wind speeds in m/sec respectively. From (5.2) it can be seen that below v_{ci} and above v_{co} WT generates zero power; below v_{ci} power in the wind is not sufficient to either overcome the friction of the drivetrain, or to yield net positive power generation, above v_{co} due to danger of mechanical failure the WT is aerodynamically slowed and stopped, and then mechanically locked into place to prevent rotation. The total power output of the HPGS is calculated as follows

$$P_H(t) = N_{pv}P_{pv}(t) + N_{wt}P_{wt}(t) \;\; \forall t > 0 \tag{5.3}$$

subject to the following constraints

$$N_{pv}^{min} \leq N_{pv} \leq N_{pv}^{max}$$

and

$$N_{wt}^{min} \leq N_{wt} \leq N_{wt}^{max}$$

where P_H is the total power output of HPGS, N_{pv} is the number of PV panels, and N_{wt} is the number number of WTs.

5.2.2 Battery Energy Storage System

The mathematical model of BES system presented in Section 4.2.3 is used.

5.2.3 Diesel Generation System Modeling

As discussed before that the power output of RE sources is unpredictable and variable, so it can happen during the operation of the MG that outputs of the HPGS and BES system become insufficient to supply the required load demand, in such events, the diesel generation system supplies the excessive demand. Instead of a single large DG unit we have assumed several smaller DG units, to enhance the overall efficiency of the system. The power output of diesel generation system is modeled as follows

$$P_{DG}(t) = \begin{cases} \sum_{i=1}^{n_{dg}} p_{dg}^{i}(t) & P_L(t) > P_H(t) + P_{BES}(t) \\ 0 & otherwise \end{cases} \quad \forall t > 0 \tag{5.4}$$

where

$$\sum_{i=1}^{n_{dg}} p_{dg}^{i}(t) = P_L(t) - P_H(t) - P_{BES}(t) \tag{5.5}$$

where P_{DG} is the total power output of diesel generation system and p_{dg}^{i} is the output power of i^{th} DG unit, n_{dg} is the total number of DGs, P_{BES} is the power output of BES system, and P_H is the output power of hybrid power generation system. From (**??**) $P_{DG} = 0$ if power output of RE sources and BES system is more than load power

demand.

5.2.4 Load Modeling

The load can be classified into two main categories: controllable load and uncontrollable load. Every home has some appliances which are devoted to users habits and their needs, for example hair dryers, cooking appliances, refrigerator, computers, lighting, etc. The load of these appliances is referred as uncontrollable load. In this study, real residential power demand data of Dammam city is used.

Similarly, in every home their are some appliances which are controllable, means that shifting their load to some extent do not affect the daily routine of the consumers. For example, water pump, dish washer, clothes dryer, washing machine, EV, etc, the load of these appliances is called controllable load. Load demand of both controllable and uncontrollable loads except the EV load are incorporated in the load power demand data of Dammam city.

In near future, due to the integration of large number EVs in the power system the load demand will increase drastically. Hence, considering the EVs load at the design stage is crucial for the reliable operation of the future power system. Currently the real EVs load is not available. However, EVs load can be approximated. In EV modeling the battery capacity, charge depleting distance, initial SOC, charging/discharging rate, and user behavior are the most important parameters [136]. The battery capacity, charge depleting distance, and charging rate can be acquired in advance. However, the user behavior may not be obtained in advance. In this research, three types of EVs, i.e., Tesla

Table 5.1: Characteristics of EVs

EV Type	Battery bank (kWh)	Charg./Disch. rate (kW)	Maximum Mileage (mi)
Tesla S70	70	11	240
Nissan Leaf	24	6.6	126
Th!nk City	24	6.6	100

S 70, Nissan Leaf, and Th!nk City are considered to make the analysis more realistic and practical. The information about the battery bank, charging rate, and maximum daily mileage of the three EVs are given in Table 5.1. The total number of EVs in the system N_{ev} can be obtained from the EV penetration level as follows:

$$N_{ev} = \sum_{c=1}^{c_t} \rho \nu_c n_h \tag{5.6}$$

where ρ, is the penetration level, ν_c is the percentage of c^{th} class of EV, c_t is the total number of EV classes, and n_h is the total number of houses. The daily mileage, departure time, arrival time, and charging time are different aspects of user behavior which can be obtained from lognormal distribution.

$$\chi_{e,c,d} = logNormal(3.375, 0.5) \tag{5.7}$$

$$\overline{\tau}_{e,c,d} = logNormal(\Lambda_{dp}, \sqrt{3}) \tag{5.8}$$

$$\underline{\tau}_{e,c,d} = logNormal(\Lambda_{ar}, \sqrt{3}) \tag{5.9}$$

where $\chi_{e,c,d}$ is the miles driven by the e^{th} vehicle of class c at day d, $\overline{\tau}$ is the departure time, $\underline{\tau}$ is the arrival time, and Λ_{dp} and Λ_{ar} are average departure and arrival times respectively. Once the miles driven are calculated, the energy needed to fully charge an EV can be estimated as described below

$$\hbar_{e,c,d} = \begin{cases} E_c^{ev} & \chi_{e,c,d} \geq \lambda_c \\ \frac{E_c^{ev}}{\lambda_c} \chi_{e,c,d} & otherwise \end{cases} \tag{5.10}$$

where $\hbar$ is the energy needed to charge an EV, E^{ev} is the battery energy capacity of EV, and λ is the charge depleting distance. The time required to charge the EV is modeled as

$$\tau_{e,c,d}^{chg} = \frac{\hbar_{e,c,d}}{p_c^{ev}} \tag{5.11}$$

where τ^{chg} is total time required to charge the EV and p_c^{ev} is the charging rate of c^{th} class of EV. It is assumed that EVs start charging right after their arrival. The EV charging load is modeled as follows

$$\xi_{e,c,d}\left(\underline{\tau}_{e,c,d} + y\right) = \begin{cases} p_c^{ev} & if\ y \leq \lfloor \tau_{e,c,d}^{chg} \rfloor \\ p_c^{ev}\left(\tau_{e,c,d}^{chg} - \lfloor \tau_{e,c,d}^{chg} \rfloor\right) & else \end{cases} \tag{5.12}$$

where

$$y = 1, 2, ..., \lfloor \tau^{chg}_{e,c,d} \rfloor + 1$$

and

$$\underline{\tau}_{e,c,d} + y > \overline{\tau}_{e,c,d}$$

where ξ is the hourly charging load of EV. The state-of-charge of an EV after charging period is estimated as given below

$$SOC_{e,c,d}(t + \Delta t) = SOC_{e,c,d}(t) + \Delta t \frac{\xi_{e,c,d}(t)}{E^{ev}_{c}} \tag{5.13}$$

where

$$SOC^{min}_{e,c,d} \leq SOC_{e,c,d} \leq SOC^{max}_{e,c,d} \tag{5.14}$$

where SOC^{ev} is the final SOC of an EV after charging. SOC^{min} and SOC^{max} are the minimum and maximum SOC of an EV battery. As EV is a controllable load so its load can be shifted. The shifted EV load is determined as following

$$\xi_{e,c,d}(t + \tau_s) = \xi_{e,c,d}(t) \;\; \forall t > 0 \tag{5.15}$$

where

$$\tau^{min}_{s} \leq \tau_s \leq \tau^{max}_{s}$$

where τ_s is the time shift. The daily EV hourly load (P^{ev}) can be calculated using

following equation

$$P_d^{ev}(t) = \sum_{c=1}^{c_t} \sum_{e=1}^{n_c^{ev}} \xi_{e,c,d}(t) \;\; \forall t > 0 \tag{5.16}$$

5.3 Problem Formulation

One of the primary reasons behind the exploitation of RE sources around the globe is global warming due to GHG emissions. RE sources has proved to be a promising solution for GHG emissions but they have high cost and pose reliability and stability problems in the power system. Hence, in order to get the full benefits of RE sources a system design is necessary, that could significantly reduce GHG emissions at reasonable cost, and should also have higher reliability and stability. The system design in this study is based upon the cost minimization, GHG emissions reduction and dump energy minimization while supplying the load demand reliably.

5.3.1 Reliability and Economic Modeling

The total power generated by the MG consists of power output of HPGS, BES system, and diesel generation system

$$P_{MG}(t) = P_H(t) + P_{BES}(t) + P_{DG}(t) \;\; \forall t > 0 \tag{5.17}$$

where P_{MG} is the total generation of MG. Energy served E_s is the sum of the load demand that is supplied by the MG system during its operation, mathematically E_s is defined as

$$E_s = \sum_{t=1}^{n} \Gamma_{es}(t) \tag{5.18}$$

where

$$\Gamma_{es}(t) = \begin{cases} P_L(t) & P_{MG}(t) \geq P_L(t) \\ & \forall t > 0 \\ P_{MG}(t) & otherwise \end{cases} \tag{5.19}$$

Energy not served E_{ns} is the sum of load demand that is not supplied by the MG during its operation.

$$E_{ns} = \sum_{t=1}^{n} \Gamma_{ens}(t) \tag{5.20}$$

where

$$\Gamma_{ens}(t) = \begin{cases} P_L(t) - P_{MG}(t) & P_L(t) > P_{MG}(t) \\ & \forall t > 0 \\ 0 & otherwise \end{cases} \tag{5.21}$$

The net discounted energy served NDE_s is calculated as

$$NDE_s = \sum_{j=0}^{n_l} \frac{1}{(1+\eth)^j} E_s \tag{5.22}$$

where n_l is the total number of years of operation and $\eth$ is the discount rate. The cost of the HPGS is modeled as follows

$$C_h = \sum_{k=1}^{n_{sc}} C_{c,sr}^k P_{sr}^k + \sum_{k=1}^{n_{sc}} \sum_{j=0}^{n_l} \sum_{t=1}^{n} \frac{F_{om,v}^k P^k(t) + T^k(t) F_{om,f}^k P_{sr}^k}{(1+\eth)^j} \tag{5.23}$$

where C_h is the total cost of hybrid generation system, $C^k_{c,sr}$ is the investment cost of the k^{th} source in $\$/MW$, P^k_{sr} is the installed capacity of k^{th} source in MW, n_{sc} is the total number of sources employed by HPGS, $F^k_{om,v}$ is the fixed operation and maintenance cost of k^{th} source in $\$/MW$, P^k is the power output of k^{th} source, and $F^k_{om,f}$ is the fixed operation and maintenance cost of k^{th} source in $\$/MW-yr$. In (5.23) the first term represents the initial investment cost and second term stands for the present worth of operation and maintenance costs. The cost of energy storage system depends on both power and energy capacity of BES system. The cost of BES system is modeled as follows

$$C_b = \sum_{l=1}^{n_{stg}} \left(C^l_{c,e} E^l_{stg} + C^l_{c,p} P^l_{stg} \right) + \sum_{l=1}^{n_{stg}} \sum_{s=\ell^i_{bat}}^{n_l - \ell^i_{bat}} \frac{C^l_{c,e} E^l_{stg} + C^l_{c,p} P^l_{stg}}{(1+\eth)^s} \tag{5.24}$$

where

$$s = \ell^i_{bat}, 2\ell^i_{bat}, 3\ell^i_{bat}, ...n_l - \ell^i_{bat}$$

where C_b is the total cost of the BES system, $C^l_{c,e}$ is the cost related to the energy capacity of l^{th} storage unit in $\$/MWh$, E^l_{stg} is the energy capacity of l^{th} storage unit in MWh, where $C^l_{c,p}$ is the cost related to the power capacity of l^{th} storage unit in $\$/MW$, P^l_{stg} is the power capacity of storage unit in MW, n_{stg} is the total number of storage units, and ℓ_{bat} is the life of the BES system. In (5.24), the first term stands for the initial investment cost of the BES system, while second term represents the present value of replacement cost of BES system. The cost associated with the diesel generation system

is modeled as following

$$C_d = \sum_{i=1}^{n_{dg}} C^i_{c,dg} P^i_{r,dg} + \sum_{i=1}^{n_d} \sum_{s=\ell^i_{dg}}^{n_l - \ell^i_{dg}} \frac{1}{(1+\eth)^s} C^i_{c,dg} P^i_{r,dg} + \sum_{i=1}^{n_{dg}} \sum_{j=0}^{n_l} \sum_{t=1}^{n} \frac{N^i_{run} M^i_{dg}}{(1+\eth)^{j-1}} \left(\Psi^i p^i_{dg}(t) + \varphi^i P^i_{r,dg} \right) f_p \tag{5.25}$$

where

$$s = \ell^i_{dg}, 2\ell^i_{dg}, 3\ell^i_{dg}, ...n_l - \ell^i_{dg}$$

where C_d is the total cost of the diesel generation system, $C^i_{c,dg}$ is investment cost of i^{th} DG unit in $\$/MW$, $P^i_{r,dg}$ is the rated capacity of i^{th} DG unit in MW, n_dg is the total number of DG units, γ^i is the life of i^{th} DG unit, N^i_{run} is the total operation time of i^{th} DG in hr, M^i_{dg} is the operation and maintenance cost of i^{th} DG in $\$/hr$, f_p is the fuel price in $\$/ltr$, P^i_{dg} is the power output of i^{th} DG, Ψ^i is the fuel curve slope coefficient of i^{th} DG unit, and φ^i is the fuel curve intercept coefficient of i^{th} DG unit. In (5.25) the first term represent the initial investment cost of diesel generation system, second term stands for the replacement cost, third term represents the present worth of the cost associated with the operation and maintenance costs and fuel cost of diesel generation system.

5.3.2 GHG Emissions Modeling

When electric power is generated by burning fossil fuels, it results in GHG emissions in the environment. There is a correction cost which is needed to mitigate the damage caused by these emissions as shown in Table 4.1. This correction cost would be a saving

if the electric power is generated by utilizing RE sources instead of fossil fuels. This saving is named as emission reduction benefit cost (ERBC), and modeled as

$$C_{erbc} = \sum_{j=0}^{n_l} \sum_{m=1}^{4} \sum_{t=1}^{n} \frac{1}{(1+\eth)^j} P_{MG}(t) E^m E_{cc}^m \tag{5.26}$$

where C_{erbc} is the total emission reduction benefit cost, E^m is the emission of m^{th} type of greenhouse gas in kg/MW, and E_{cc}^m is the correction cost associated with the m^{th} type of greenhouse gas in $\$/kg$.

5.3.3 Dump Energy Modeling

As the outputs of RE sources are uncontrollable and stochastic, it is possible during the operation that the output of RE sources become higher than the load demand and BES maximum watt capacity. During such events the surplus energy should be dumped for stable operation of MG. The cost of dump energy is calculated using the following equation

$$C_{dmp} = \sum_{t=1}^{n} \sum_{j=0}^{n_l} \frac{1}{(1+\eth)^j} \left(\mu \frac{\alpha}{\alpha+\beta} \Upsilon(t) + \sigma \frac{\beta}{\alpha+\beta} \Upsilon(t) \right) \tag{5.27}$$

where α is the installed capacity of PV, β is the installed capacity of WT, μ is the cost per unit of PV, σ is the cost per unit of WT, and Υ is the dump energy. For simplicity, it is assumed that the total dump energy is equally coming from WT and PV.

5.3.4 Cost Function Formulation

The objective is to find an optimal combination of PV, WT, BES system, and DG that must supply the complete load demand with lower cost, lower GHG emissions, lower dump energy. The objective function of the optimization problem is formulated as follows

$$obj: J = \sqrt{\left(J_1(\boldsymbol{X}) + J_2(\boldsymbol{X}) - J_3(\boldsymbol{X})\right)^2} \rightarrow \min \tag{5.28}$$

$$s.t. \begin{cases} \boldsymbol{g}_\ell(\boldsymbol{X}) = 0 \quad \ell = 1,2,,...,m \\ \boldsymbol{h}_\iota(\boldsymbol{X}) \leq 0 \quad \iota = 1,2,,...,q \end{cases} \tag{5.29}$$

where

$$\boldsymbol{X} = \left[N_{PV},\, N_{WT},\, E_{stg},\, P_{stg}, P_{r,dg}\right] \tag{5.30}$$

The first term in the objective function is the total cost of the MG. The total cost of HPGS (5.23), BES system (5.24), and diesel generation system (5.25) is incorporated in the first term of (5.28). The second term of the objective function represents the cost of dump energy (5.27), while the last term represents the GHG emissions that are translated in terms of cost using ERBC (5.26) concept as discussed in Section 5.3.2. The equality constraints are represented by $\boldsymbol{g}$ and in-equality constraints are presented by $\boldsymbol{h}$. All system constraints are listed as follows:

The Primary System Constraint (Generation = Demand):

$$P_H(t) + P_{BES}(t) + P_{DG}(t) - P_L(t) = 0 \ \ \forall t > 0 \tag{5.31}$$

The hybrid generation system constraints:

$$N_{PV}^{min} \leq N_{PV} \leq N_{PV}^{max} \tag{5.32}$$

$$N_{WT}^{min} \leq N_{WT} \leq N_{WT}^{max} \tag{5.33}$$

Battery energy storage system Constraints:

$$0 \leq P_{BES}^{c}(t) \leq P_{BES}^{cmax} \ \ \forall t > 0 \tag{5.34}$$

$$0 \leq P_{BES}^{d}(t) \leq P_{BES}^{dmax} \ \ \forall t > 0 \tag{5.35}$$

$$E_{BES}^{min} \leq E_{BES}(t) \leq E_{BES}^{max} \ \ \forall t > 0 \tag{5.36}$$

Diesel generation system constraints:

$$\sum_{i=1}^{n_{dg}} p_{dg}^{i}(t) = 0 \ \ if: \ P_L(t) \leq P_H(t) + P_{BES}(t) \ \ \forall t > 0 \tag{5.37}$$

$$\begin{aligned} \sum_{i=1}^{n_{dg}} p_{dg}^{i}(t) =& P_L(t) - P_H(t) - P_{BES}(t) \\ & if: \ P_L(t) \geq P_H(t) + P_{BES}(t) \ \ \forall t > 0 \end{aligned} \tag{5.38}$$

EV load constraints:

$$SOC^{min} \leq SOC(t) \leq SOC^{max} \quad \forall t > 0 \tag{5.39}$$

$$P^{ev}_{min} \leq P^{ev}(t) \leq P^{ev}_{max} \quad \forall t > 0 \tag{5.40}$$

5.4 Databases

The solar PV and WT are modeled as discussed in Section 5.2.1 and their power outputs are calculated using the solar irradiation and wind speed data, spanning a length of one year with a resolution of one hour. The power outputs of WT and PV are shown in Fig. 5.4 and Fig. 5.5. The solar PV generates power during the day time only and its power increases to maximum from morning to noon and decreasing trend can be observed afterward. The output power of WT fluctuates throughout the day without following any pattern. Similarly, the controllable load is modeled as given in Section 5.2.4. A community load power demand which consists of EV load and residential load is shown in Fig. 5.6. The EV owners are expected to reach home around 6 pm, after reaching home the owners start charging their EVs. It can be observed that residential load peak appear around 8 pm. Since, solar PV cannot generate power during the night time, hence supplying this type of load by utilizing RE sources and storage only may result in a very high cost.

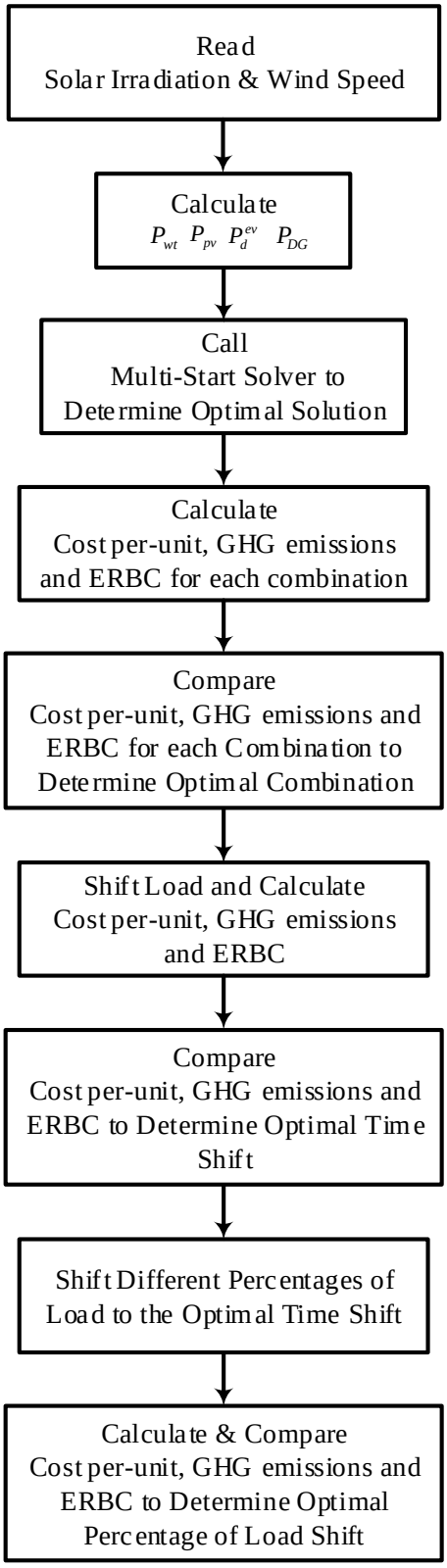

Figure 5.3: Flow chart of proposed methodology.

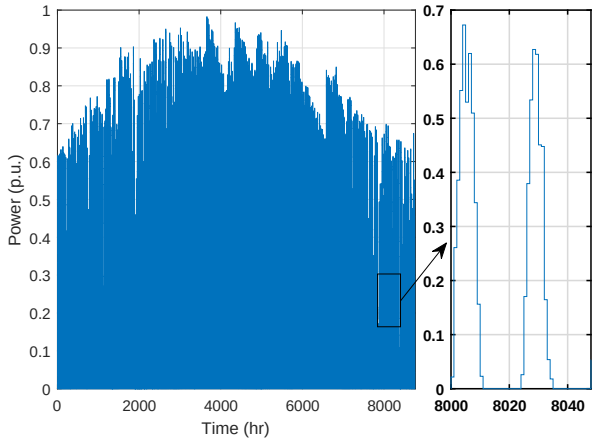

Figure 5.4: Power output of solar power generation system of one calender year.

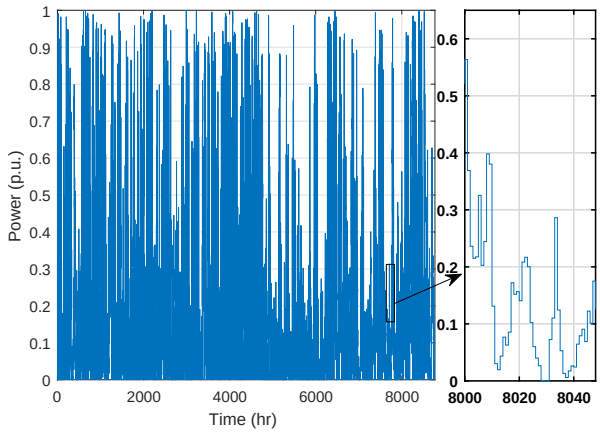

Figure 5.5: Power output of wind power generation system of one calender year.

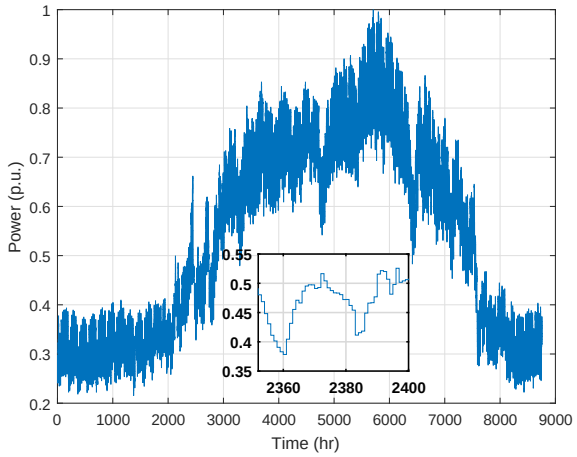

Figure 5.6: Community load power demand spanning a calender year.

5.5 Results and Discussions

Since the future grid is becoming decentralized, we consider the scenario of an standalone MG. The design of a MG employing RE sources is site dependent and varies from one geographical location to another depending on the local available resources and load demand and their behavior. Different geographical locations may require different combinations of distributed generators and ESS. So, it is vital to check different types of available solutions in order to supply the load efficiently and economically. In this study, the following six different topologies for MG the design are considered:

- CASE-I: PV-WT-BES-DG based MG
- CASE-II: WT-BES-DG based MG
- CASE-III: WT-DG based MG
- CASE-IV: PV-DG based MG
- CASE-V: PV-WT-DG based MG
- CASE-VI: PV-BES-DG based MG

The capacity optimization of these topologies are done using the cost function as in Section 5.3.4. The capacities that correspond to the optimal solution are tabulated in Table 5.2. The cost, reliability (energy served) and GHG emissions have special significance in assessing the performance of a MG employing both RE sources and conventions generators. It is always desired that a system should have lower cost, higher reliability and lesser GHG emissions. The cost per-unit of the six MG topologies

Table 5.2: Optimal Capacities of Different MG Topologies

Case Index	PV (MW)	WT (MW)	BES (MWh)	BES (MW)	DG (MW)
CASE-I	13.86	7	23.76	4.75	10.0
CASE-II	0	10.4	18.53	3.71	10.0
CASE-III	0	8	0.00	0.00	10.0
CASE-IV	11.17	0	0.00	0.00	11.0
CASE-V	10.0	6.04	0.00	0.00	10.0
CASE-VI	23.62	0.0	48.25	9.65	8.00

is presented in Fig. 5.7a. The term cost per-unit incorporates both cost and reliability indices in it. It can be seen that per-unit cost is minimum for CASE-I in which all available sources are utilized, while cost is maximum for CASE-IV in which only PV and DG are employed.

As one of the primary purposes behind the utilization of RE sources in the power system is to reduce the GHG emissions by supplying clean energy. The variation in GHG emissions of the six MG topologies is shown in Fig. 5.7b. The GHG emissions are minimum for CASE-VI as the overall installed capacities of RE sources and BES system are maximum for this case and the DG size is also smallest for this case. While the GHG emissions are maximum for CASE-IV because in this case the only RE source i.e., PV is employed, which supplies the load demand during the day time only, while during the night DG is utilized to supply the demand completely which results in higher GHG emissions. A comparison based on ERBC and clean energy (energy from RE sources and BES system) supplied by the six MG topologies are shown in Fig. 5.7c and Fig. 5.7d respectively. The clean energy served and ERBC are maximum for CASE-

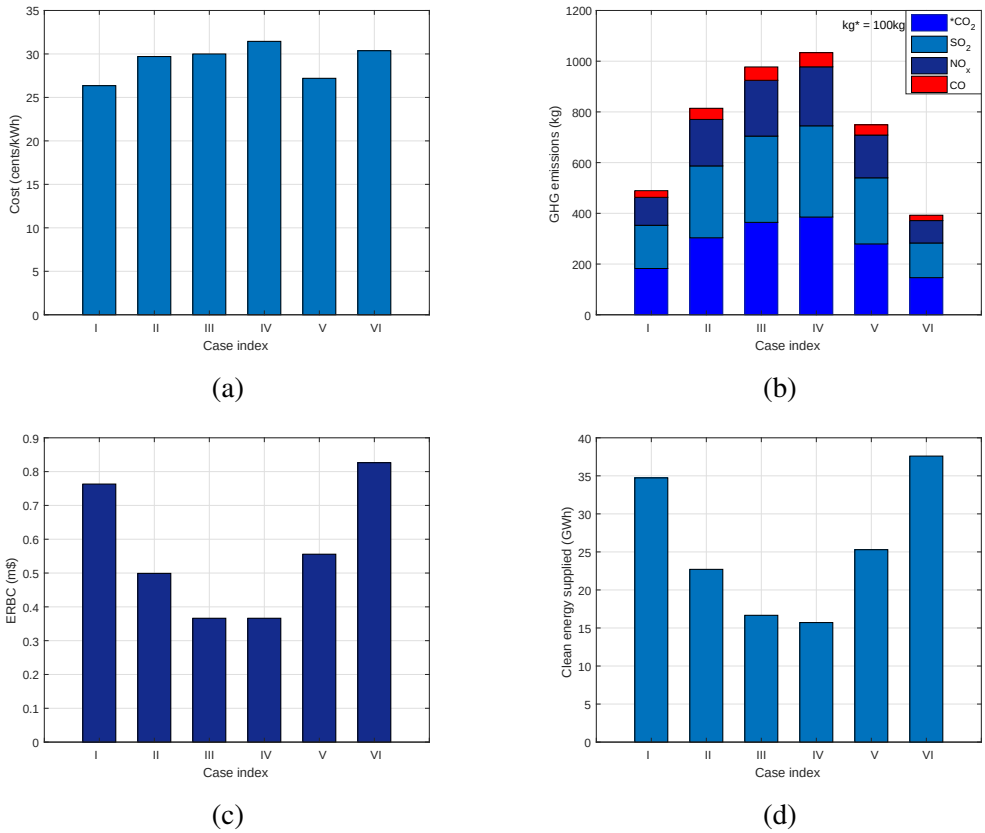

Figure 5.7: (a) Cost per-unit of the six MG topologies (b) GHG emissions comparison of the six MG topologies (c) ERBC comparison of the six MG topologies (d) Clean energy served by the six MG topologies

VI because the overall installed capacities of RE sources and BES system are highest. While ERBC and clean energy supplied are least for CASE-IV.

A MG having lower cost, higher reliability, lesser GHG emissions, higher clean energy, and higher ERBC can be considered as a promising solution. The best topology from the possible solutions is selected by carrying out the sensitivity analysis based upon the per-unit cost, GHG emissions, ERBC, and clean energy served by the system. When comparing CASE-I and CASE-II, it can be observed that CASE-I has lower cost, lower GHG emissions, higher ERBC and higher clean energy which make CASE-I a better solution as compared to CASE-II. Similarly, the cost and GHG emissions are

Table 5.3: Optimal Capacities for Different Time Shifts

Shift (hr)	PV (MW)	WT (MW)	BES (MWh)	BES (MW)	DG (MW)
0	13.86	7.00	23.76	4.75	10.0
1	13.8	6.70	24.43	4.87	10.0
2	14.8	7.66	25.51	5.10	10.0
3	18.0	6.58	35.10	7.02	10.0
-1	20.0	4.40	32.24	6.45	9.00
-2	17.8	5.55	26.50	5.30	8.00
-3	14.6	6.12	16.55	3.30	8.00

lower and ERBC and clean energy are higher for CASE-I as compared to CASE-III, CASE-IV and CASE-V. The GHG emissions for CASE-VI are lesser than CASE-I but its cost is significantly higher. Hence, from the previous analysis it can be concluded that CASE-I is the better option. It is important to note that these results can not be generalized for every location. As mentioned earlier, the design of a MG exploiting conventional and RE distributed generators is site dependent. So, before installing distributed generators feasibility study of several possible solutions should be carried out to determine the best techno-economical solution.

The innovations in power electronics and the introduction of the advance high-speed information and communication technologies and sophisticated control has made the load demand of the power system more flexible and easily controllable. In order to highlight the impact of load shifting on the cost, GHG emissions, ERBC, clean energy supplied by the system, the load demand is shifted. The cost function for the MG topology given in CASE-I is solved for different load shifts and the optimal capacities

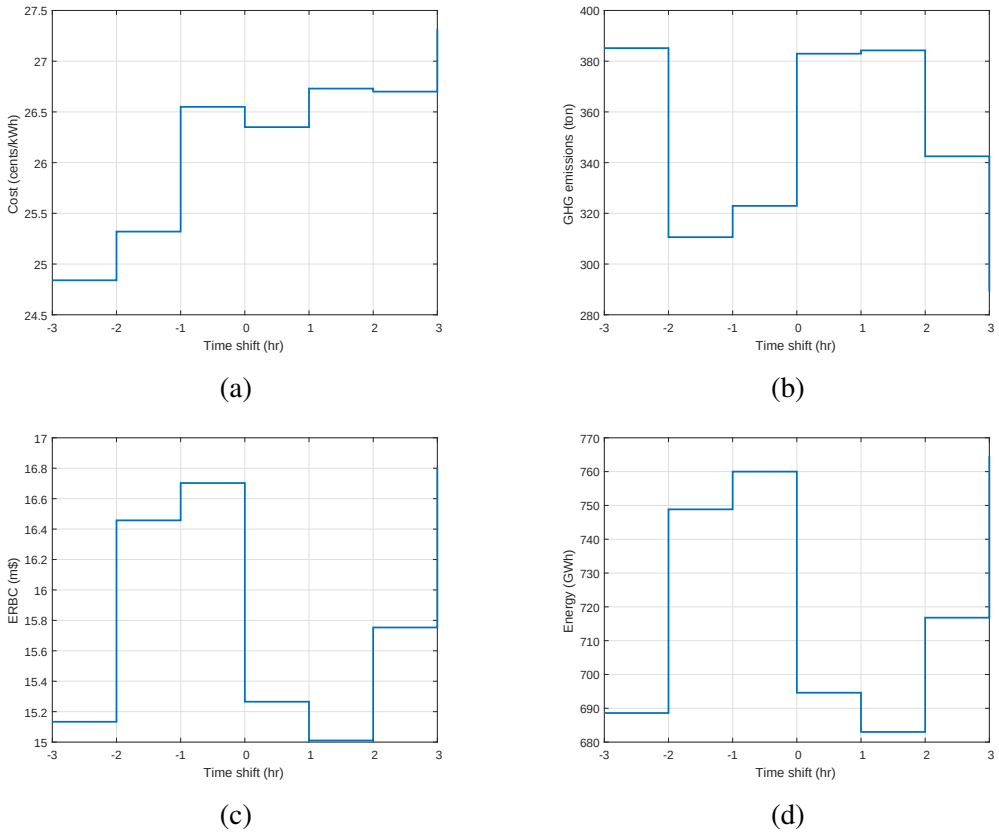

Figure 5.8: (a) Variation in cost per-unit w.r.t load shift (b) GHG emissions vs load shifting (c) ERBC vs load shifting (d) Clean energy served vs load shifting

determined are tabulated in Table 5.3. As the load has typical residential load behaviour due to which peak demand appears in the evening time and shifting the load towards the day time results in a decrease in capacities of DG.

The variation in cost per-unit with the load shift is shown in Fig. 5.8a. The cost per-unit is minimum for the shift -3 hours and maximum for the shift of 3 hours. Shifting the load by -3 hours results in the efficient utilization of BES system and RE sources which resulted in lower cost. The variation in GHG emissions with the load shift is shown in Fig. 5.8b. The GHG emissions are lowest for a load shift of 3 hours as for this case the installed capacity of RE sources and BES system are highest, similarly the

Table 5.4: Optimal Capacities For Different Percentages of Time Shift

Shift (%)	PV (MW)	WT (MW)	BES (MWh)	BES (MW)	DG (MW)
100	14.60	6.12	16.55	3.30	8.0
80	16.50	5.50	21.54	4.31	8.0
60	16.65	6.00	22.00	4.4	8.0
40	17.60	6.00	23.60	4.72	8.0
20	16.00	5.80	21.10	4.22	8.0

GHG emissions are also lower for the load shift of -1 hour. The variations is ERBC and clean energy served are shown in Fig. 5.8c and Fig. 5.8d respectively. Both ERBC and clean energy supplied are maximum for a shift of 3 hours and minimum for a shift of 1 hour, as the installed capacities of RE sources and BES system are lowest for a shift of 1 hour.

The determination of the best time shift depends upon the priorities of the installing authority. If the priority is GHG emissions then the combination that corresponds to the shift of 3 hours can be taken as best solution. But if the the priority is the cost then the capacities of PV, WT, BES, and DG corresponding to the shift of -3 can be taken as best solution. As the combination corresponding to -3 hours shift gives the lowest cost and supplies the load at 68% lesser emissions as compared to the conventional generation so it can be taken as best solution among the available options.

Sometimes it is difficult to shift the 100% of the load demand due to the presence of uncontrollable appliances. To study the impact of shifting different percentages of the total load demand on the installed capacities, cost, GHG emissions, ERBC, and clean

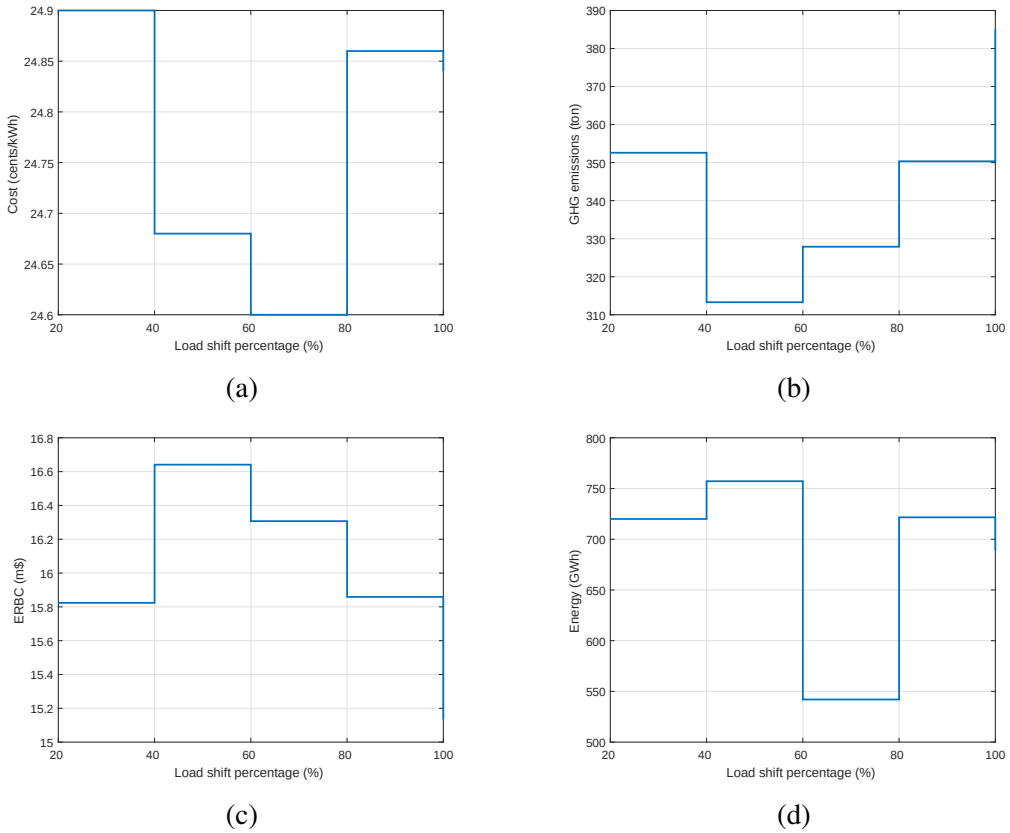

Figure 5.9: (a) Variation in cost per-unit w.r.t different percentages of load shift (b) GHG emissions vs percentages of load shift (c) ERBC vs percentages of load shift (d) Clean energy served vs percentages of load shift

energy served by the system, different percentages of the total load are shifted by -3 hours. The capacities that correspond to different different percentage of load shifts are tabulated in Table 5.4.

The variation in per-unit cost with the different percentages of load shift is presented in Fig. 5.9a. It can be observed that cost is minimum for a shift of 60% of load and maximum for 20% of load shift. Even the shift of only 20% of the load by -3 hours can result in the considerable saving as compared to no shift. The variation in GHG emissions, ERBC, and clean energy supplied are shown in Fig. 5.9b, Fig. 5.9c, and Fig. 5.9d.

From the above analysis it can be concluded that shifting the load demand can result in cost reduction, GHG emissions reduction, savings in terms of ERBC and increase the green energy share. As it can be observed that shifting only 20% of the total load demand resulted in 5.5% reduction in per unit cost. It is important be noted that this reduction can actually result in huge savings as this is the reduction in one unit and this small system is serving more than 1000 GWh during its life time. Similarly, the GHG emissions are 7.9% lesser when 20% of the total load shifted by -3 hours. Moreover, it can be observed that shifting the load also benefits in terms of ERBC and clean energy supplied by the system.

Any small residential community, cite office of a company, or even a single home can benefit from the proposed methodology. As in the aforementioned systems the load control is easier that is why utilizing the proposed methodology these systems can get maximum benefits in terms of cost, GHG emissions, ERBC and clean energy. The proposed methodology is also applicable for the large systems but in the large systems the load control is difficult as compared to the small systems.

CHAPTER 6

CONCLUSION

A technique for the capacity optimization of RE sources, i.e., WT and solar PV and associated BESS in grid-connected MG system has been proposed (see Chapter 3). The optimal capacities are determined based on the energy served to cost per unit ratio. It has been shown that the optimal solution is economical and produces less CO_2 emissions. A comparison based on the cost and emissions for some selected cases is also presented and it is proved that the optimal solution is superior over the other solutions. The significance of the proposed method lies in the fact that it eschews under-sizing and over-sizing because it searches every possible solution. Also, to make the methodology more practical, forced outage rates of WT and PV and utilization factor of BESS are considered. The proposed methodology is quite general and it can be extended to other types of generation and storage technologies and also equally valid for any geographical location.

A methodology for joint capacity optimization of hybrid renewable power generation system and energy storage in the context of a grid-connected microgrid (MG) has

also been presented (see Chapter 4). The hybrid generation system is comprised of solar photovoltaic (PV) and wind turbine (WT) and hybrid energy storage system (HESS) is composed of battery energy storage (BES) system and supercapacitor (SC) technology. The combined optimization exploits the benefits of both hybrid power generation and HESS. The proposed strategy is primarily based upon a few important factors associated with a MG system such as cost minimization, greenhouse gases (GHG) emissions reduction, higher emission reduction benefit cost (ERBC), and higher reliability. The optimization problem has been formulated and solved in a piece-wise fashion to decrease the complexity and computational time.

The proposed methodology has been tested using real residential power demand, solar irradiation and wind speed data. The resulted optimal solution is economical, has higher reliability and lesser GHG emissions when compared with other possible solutions. It has also been shown that when the MG is operated with optimal parameters it serves the demand effectively. Moreover, a comparison between three case studies, i.e., PV/WT/BES/SC, PV/WT/BES, and conventional generation has also been presented. It has been observed that the topology, PV/WT/BES/SC, resulted in the optimal choice as there are multiple benefits associated with hybrid BES-SC energy storage system. It is an economical and reliable solution because the use of SC in conjunction with BES prolongs the BES lifespan, and supplies the demand more effectively and efficiently. In addition, it results in least GHG emissions thus increasing ERBC which makes the overall system more economical and eco-friendly.

An improved methodology for the capacity optimization a typical residential MG

employing PV, WT, BES, and DG in six different topologies, i.e., PV-WT-BES-DG, PV-WT-DG, WT-DG-BES, WT-DG, PV-BES-DG, and PV-DG, has been presented to supply a residential load demand comprising of house and EV load demand (see Chapter 5). The capacity optimization is done based upon the initial investment cost, replacement cost, operation cost, maintenance cost, dump energy cost, and GHG emissions. The multi-objective optimization problem is formulated and solved innovatively in the presence of various realistic constraints from RE sources generation system, BES system, diesel generation system, and EV load. As a case study the proposed methodology is tested using the real load power demand, wind speed, and solar irradiation data. A comparison based upon the cost per unit, GHG emissions, and ERBC has been presented for the six topologies. It has been observed that the topology PV-WT-BES-DG is not only economical but also more reliable, has lesser emissions which makes it more environmental friendly, and higher ERBC.

Furthermore, the impact of load shifting on the cost, GHG emissions, ERBC and clean energy supplied by system has been studied. It has been observed that shifting a small percentage of total load can result in considerable saving in terms of cost. Moreover, it has been observed that GHG emissions can be reduced and ERBC and clean energy supplied by the MG can be increased by shifting the load demand.

REFERENCES

[1] E. Kuznetsova, C. Ruiz, Y.-F. Li, and E. Zio, "Analysis of robust optimization for decentralized microgrid energy management under uncertainty," *International Journal of Electrical Power & Energy Systems*, vol. 64, pp. 815–832, 2015.

[2] N. Hatziargyriou *et al.*, *Microgrids: architectures and control*. Wiley Online Library, 2014.

[3] J. O. Dada, "Towards understanding the benefits and challenges of smart/micro-grid for electricity supply system in nigeria," *Renewable and Sustainable Energy Reviews*, vol. 38, pp. 1003–1014, 2014.

[4] C. Schwaegerl and L. Tao, "Quantification of technical, economic, environmental and social benefits of microgrid operation," *Microgrids: Architectures and control*, pp. 275–313, 2014.

[5] A. Khodaei, "Provisional microgrid planning," *IEEE Transactions on Smart Grid*, vol. 8, no. 3, pp. 1096–1104, 2017.

[6] K. Zhou, S. Yang, Z. Chen, and S. Ding, "Optimal load distribution model of microgrid in the smart grid environment," *Renewable and Sustainable Energy Reviews*, vol. 35, pp. 304–310, 2014.

[7] D. Feldman, "Photovoltaic (pv) pricing trends: historical, recent, and near-term projections," 2014.

[8] R. Fu, D. J. Feldman, R. M. Margolis, M. A. Woodhouse, and K. B. Ardani, "Us solar photovoltaic system cost benchmark: Q1 2017," National Renewable Energy Laboratory (NREL), Golden, CO (United States), Tech. Rep., 2017.

[9] A. Arabali, M. Ghofrani, M. Etezadi-Amoli, and M. S. Fadali, "Stochastic performance assessment and sizing for a hybrid power system of solar/wind/energy storage," *IEEE Transactions on Sustainable Energy*, vol. 5, no. 2, pp. 363–371, 2014.

[10] W. Su, J. Wang, and J. Roh, "Stochastic energy scheduling in microgrids with intermittent renewable energy resources," *IEEE Transactions on Smart Grid*, vol. 5, no. 4, pp. 1876–1883, 2014.

[11] W. Zhou, C. Lou, Z. Li, L. Lu, and H. Yang, "Current status of research on optimum sizing of stand-alone hybrid solar–wind power generation systems," *Applied Energy*, vol. 87, no. 2, pp. 380–389, 2010.

[12] A. Kyritsis, D. Voglitsis, N. Papanikolaou, S. Tselepis, C. Christodoulou, I. Gonos, and S. Kalogirou, "Evolution of PV systems in Greece and review

of applicable solutions for higher penetration levels," *Renewable Energy*, vol. 109, pp. 487–499, 2017.

[13] H. T. Le and T. Q. Nguyen, "Sizing energy storage systems for wind power firming: An analytical approach and a cost-benefit analysis," in *Power and Energy Society General Meeting - Conversion and Delivery of Electrical Energy in the 21st Century*. IEEE, 2008, pp. 1–8.

[14] P. Denholm and R. M. Margolis, "Evaluating the limits of solar photovoltaics (PV) in electric power systems utilizing energy storage and other enabling technologies," *Energy Policy*, vol. 35, no. 9, pp. 4424–4433, 2007.

[15] B. Yang, Y. Makarov, J. Desteese, V. Viswanathan, P. Nyeng, B. McManus, and J. Pease, "On the use of energy storage technologies for regulation services in electric power systems with significant penetration of wind energy," in *5th International Conference on European Electricity Market*. IEEE, 2008, pp. 1–6.

[16] A. Khatamianfar, M. Khalid, A. V. Savkin, and V. G. Agelidis, "Improving wind farm dispatch in the Australian electricity market with battery energy storage using model predictive control," *IEEE Transactions on Sustainable Energy*, vol. 4, no. 3, pp. 745–755, 2013.

[17] M. Khalid and A. Savkin, "A model predictive control approach to the problem of wind power smoothing with controlled battery storage," *Renewable Energy*, vol. 35, no. 7, pp. 1520–1526, 2010.

[18] M. Aneke and M. Wang, "Energy storage technologies and real life applications–a state of the art review," *Applied Energy*, vol. 179, pp. 350–377, 2016.

[19] A. V. Savkin, M. Khalid, and V. G. Agelidis, "A constrained monotonic charging/discharging strategy for optimal capacity of battery energy storage supporting wind farms," *IEEE Transactions on Sustainable Energy*, vol. 7, no. 3, pp. 1224–1231, 2016.

[20] M. Khalid, A. Ahmadi, A. V. Savkin, and V. G. Agelidis, "Minimizing the energy cost for microgrids integrated with renewable energy resources and conventional generation using controlled battery energy storage," *Renewable Energy*, vol. 97, pp. 646–655, 2016.

[21] T. Ma, H. Yang, and L. Lu, "Development of hybrid battery–supercapacitor energy storage for remote area renewable energy systems," *Applied Energy*, vol. 153, pp. 56–62, 2015.

[22] M.-E. Choi, S.-W. Kim, and S.-W. Seo, "Energy management optimization in a battery/supercapacitor hybrid energy storage system," *IEEE Transactions on Smart Grid*, vol. 3, no. 1, pp. 463–472, 2012.

[23] X. Hu, L. Johannesson, N. Murgovski, and B. Egardt, "Longevity-conscious dimensioning and power management of the hybrid energy storage system in a fuel cell hybrid electric bus," *Applied Energy*, vol. 137, pp. 913–924, 2015.

[24] W. Li, G. Joós, and J. Bélanger, "Real-time simulation of a wind turbine generator coupled with a battery supercapacitor energy storage system," *IEEE Transactions on Industrial Electronics*, vol. 57, no. 4, pp. 1137–1145, 2010.

[25] A. Kuperman, I. Aharon, S. Malki, and A. Kara, "Design of a semiactive battery-ultracapacitor hybrid energy source," *IEEE Transactions on Power Electronics*, vol. 28, no. 2, pp. 806–815, 2013.

[26] M. Glavin and W. Hurley, "Optimisation of a photovoltaic battery ultracapacitor hybrid energy storage system," *Solar Energy*, vol. 86, no. 10, pp. 3009–3020, 2012.

[27] Z. Amjadi and S. S. Williamson, "Prototype design and controller implementation for a battery-ultracapacitor hybrid electric vehicle energy storage system," *IEEE Transactions on Smart grid*, vol. 3, no. 1, pp. 332–340, 2012.

[28] A. Schneuwly, "High reliability power backup with advanced energy storage (white paper)," Maxwell Technologies ,San Diego, CA, USA,, Tech. Rep., 2006.

[29] Q. Xu, X. Hu, P. Wang, J. Xiao, P. Tu, C. Wen, and M. Y. Lee, "A decentralized dynamic power sharing strategy for hybrid energy storage system in autonomous DC microgrid," *IEEE Transactions on Industrial Electronics*, vol. 64, no. 7, pp. 5930–5941, 2017.

[30] J. Shen and A. Khaligh, "A supervisory energy management control strategy in a battery/ultracapacitor hybrid energy storage system," *IEEE Transactions on Transportation Electrification*, vol. 1, no. 3, pp. 223–231, 2015.

[31] Y. Liu, W. Du, L. Xiao, H. Wang, S. Bu, and J. Cao, "Sizing a hybrid energy storage system for maintaining power balance of an isolated system with high penetration of wind generation," *IEEE Transactions on Power Systems*, vol. 31, no. 4, pp. 3267–3275, 2016.

[32] S. Zhang, R. Xiong, and J. Cao, "Battery durability and longevity based power management for plug-in hybrid electric vehicle with hybrid energy storage system," *Applied Energy*, vol. 179, pp. 316–328, 2016.

[33] J. M. Blanes, R. Gutiérrez, A. Garrigós, J. L. Lizán, and J. M. Cuadrado, "Electric vehicle battery life extension using ultracapacitors and an FPGA controlled interleaved buck–boost converter," *IEEE Transactions on Power Electronics*, vol. 28, no. 12, pp. 5940–5948, 2013.

[34] B. Hredzak, V. G. Agelidis, and M. Jang, "A model predictive control system for a hybrid battery-ultracapacitor power source," *IEEE Transactions on Power Electronics*, vol. 29, no. 3, pp. 1469–1479, 2014.

[35] M.-E. Choi, S.-W. Kim, and S.-W. Seo, "Energy management optimization in a battery/supercapacitor hybrid energy storage system," *IEEE Transactions on Smart Grid*, vol. 3, no. 1, pp. 463–472, 2012.

[36] Y.-S. Kim, E.-S. Kim, and S.-I. Moon, "Frequency and voltage control strategy of standalone microgrids with high penetration of intermittent renewable generation systems," *IEEE Transactions on Power systems*, vol. 31, no. 1, pp. 718–728, 2016.

[37] L. A. de Souza Ribeiro, O. R. Saavedra, S. L. De Lima, and J. G. De Matos, "Isolated micro-grids with renewable hybrid generation: The case of lençóis island," *IEEE Transactions on Sustainable Energy*, vol. 2, no. 1, pp. 1–11, 2011.

[38] Y. Kuang, Y. Zhang, B. Zhou, C. Li, Y. Cao, L. Li, and L. Zeng, "A review of renewable energy utilization in islands," *Renewable and Sustainable Energy Reviews*, vol. 59, pp. 504–513, 2016.

[39] T. Ma, H. Yang, and L. Lu, "A feasibility study of a stand-alone hybrid solar–wind–battery system for a remote island," *Applied Energy*, vol. 121, pp. 149–158, 2014.

[40] H. A. Kazem and T. Khatib, "A novel numerical algorithm for optimal sizing of a photovoltaic/wind/diesel generator/battery microgrid using loss of load probability index," *International Journal of Photoenergy*, vol. 2013, 2013.

[41] A. Arulampalam, N. Mithulananthan, R. Bansal, and T. Saha, "Micro-grid control of pv-wind-diesel hybrid system with islanded and grid connected operations," in *nternational Conference on Sustainable Energy Technologies (ICSET),I*. IEEE, 2010, pp. 1–5.

[42] S. C. Davis, S. E. Williams, and R. G. Boundy, "Transportation energy data book: Edition 35," Oak Ridge National Laboratory (ORNL), Oak Ridge, TN (United States), Tech. Rep., 2016.

[43] M. I. Piecyk and A. C. McKinnon, "Forecasting the carbon footprint of road freight transport in 2020," *International Journal of Production Economics*, vol. 128, no. 1, pp. 31–42, 2010.

[44] W. R. Morrow, K. S. Gallagher, G. Collantes, and H. Lee, "Analysis of policies to reduce oil consumption and greenhouse-gas emissions from the us transportation sector," *Energy Policy*, vol. 38, no. 3, pp. 1305–1320, 2010.

[45] R. T. Doucette and M. D. McCulloch, "Modeling the prospects of plug-in hybrid electric vehicles to reduce co 2 emissions," *Applied Energy*, vol. 88, no. 7, pp. 2315–2323, 2011.

[46] T. Sousa, H. Morais, Z. Vale, P. Faria, and J. Soares, "Intelligent energy resource management considering vehicle-to-grid: A simulated annealing approach," *IEEE Transactions on Smart Grid*, vol. 3, no. 1, pp. 535–542, 2012.

[47] A. Y. Saber and G. K. Venayagamoorthy, "Resource scheduling under uncertainty in a smart grid with renewables and plug-in vehicles," *IEEE systems journal*, vol. 6, no. 1, pp. 103–109, 2012.

[48] K. H. Youssef, "Power quality constrained optimal management of unbalanced smart microgrids during scheduled multiple transitions between grid-connected and islanded modes," *IEEE Transactions on Smart Grid*, vol. 8, no. 1, pp. 457–464, 2017.

[49] S. Park, J. Lee, S. Bae, G. Hwang, and J. K. Choi, "Contribution-based energy-trading mechanism in microgrids for future smart grid: A game theoretic ap-

proach," *IEEE Transactions on Industrial Electronics*, vol. 63, no. 7, pp. 4255–4265, 2016.

[50] A. A. Khan, M. H. Rehmani, and M. Reisslein, "Cognitive radio for smart grids: Survey of architectures, spectrum sensing mechanisms, and networking protocols," *IEEE Communications Surveys & Tutorials*, vol. 18, no. 1, pp. 860–898, 2016.

[51] V. C. Gungor, D. Sahin, T. Kocak, S. Ergut, C. Buccella, C. Cecati, and G. P. Hancke, "Smart grid technologies: Communication technologies and standards," *IEEE Transactions on Industrial Informatics*, vol. 7, no. 4, pp. 529–539, 2011.

[52] S. E. D. Coalition, "The demand response snap shot: The reality for demand response providers working in europe today," *Smart Energy Demand Coalition*, 2011.

[53] J. M. Morales, A. J. Conejo, H. Madsen, P. Pinson, and M. Zugno, *Integrating renewables in electricity markets: operational problems*. Springer Science & Business Media, 2013, vol. 205.

[54] C.-H. Lo and N. Ansari, "The progressive smart grid system from both power and communications aspects," *IEEE Communications Surveys & Tutorials*, vol. 14, no. 3, pp. 799–821, 2012.

[55] W. Kempton and J. Tomić, "Vehicle-to-grid power implementation: From stabilizing the grid to supporting large-scale renewable energy," *Journal of power sources*, vol. 144, no. 1, pp. 280–294, 2005.

[56] T. Wu, Q. Yang, Z. Bao, and W. Yan, "Coordinated energy dispatching in microgrid with wind power generation and plug-in electric vehicles," *IEEE Transactions on Smart Grid*, vol. 4, no. 3, pp. 1453–1463, 2013.

[57] L. Xu, X. Ruan, C. Mao, B. Zhang, and Y. Luo, "An improved optimal sizing method for wind-solar-battery hybrid power system," *IEEE Transactions on Sustainable Energy*, vol. 4, no. 3, pp. 774–785, 2013.

[58] M. Sharafi and T. Y. ELMekkawy, "Multi-objective optimal design of hybrid renewable energy systems using PSO-simulation based approach," *Renewable Energy*, vol. 68, pp. 67–79, 2014.

[59] M. Alsayed, M. Cacciato, G. Scarcella, and G. Scelba, "Multicriteria optimal sizing of photovoltaic-wind turbine grid connected systems," *IEEE Transactions on Energy Conversion*, vol. 28, no. 2, pp. 370–379, 2013.

[60] G. Ma, G. Xu, Y. Chen, and R. Ju, "Multi-objective optimal configuration method for a standalone wind–solar–battery hybrid power system," *IET Renewable Power Generation*, vol. 11, no. 1, pp. 194–202, 2016.

[61] A. Kamjoo, A. Maheri, A. M. Dizqah, and G. A. Putrus, "Multi-objective design under uncertainties of hybrid renewable energy system using NSGA-II and chance constrained programming," *International Journal of Electrical Power & Energy Systems*, vol. 74, pp. 187–194, 2016.

[62] R. Dufo-López, I. R. Cristóbal-Monreal, and J. M. Yusta, "Optimisation of PV-wind-diesel-battery stand-alone systems to minimise cost and maximise human

development index and job creation," *Renewable Energy*, vol. 94, pp. 280–293, 2016.

[63] J. Chen, W. Zhang, J. Li, W. Zhang, Y. Liu, B. Zhao, and Y. Zhang, "Optimal sizing for grid-tied microgrids with consideration of joint optimization of planning and operation," *IEEE Transactions on Sustainable Energy*, 2017.

[64] C. S. Lai and M. D. McCulloch, "Sizing of stand-alone solar PV and storage system with anaerobic digestion biogas power plants," *IEEE Transactions on Industrial Electronics*, vol. 64, no. 3, pp. 2112–2121, 2017.

[65] T. Dragičević, H. Pandžić, D. Škrlec, I. Kuzle, J. M. Guerrero, and D. S. Kirschen, "Capacity optimization of renewable energy sources and battery storage in an autonomous telecommunication facility," *IEEE Transactions on Sustainable Energy*, vol. 5, no. 4, pp. 1367–1378, 2014.

[66] A. Ogunjuyigbe, T. Ayodele, and O. Akinola, "Optimal allocation and sizing of PV/Wind/Split-diesel/Battery hybrid energy system for minimizing life cycle cost, carbon emission and dump energy of remote residential building," *Applied Energy*, vol. 171, pp. 153–171, 2016.

[67] M. H. Moradi, M. Eskandari, and S. M. Hosseinian, "Operational strategy optimization in an optimal sized smart microgrid," *IEEE Transactions on Smart Grid*, vol. 6, no. 3, pp. 1087–1095, 2015.

[68] H. Lotfi and A. Khodaei, "Hybrid AC/DC microgrid planning," *Energy*, vol. 118, pp. 37–46, 2017.

[69] R. Hosseinalizadeh, H. Shakouri, M. S. Amalnick, and P. Taghipour, "Economic sizing of a hybrid (PV–WT–FC) renewable energy system (HRES) for stand-alone usages by an optimization-simulation model: case study of iran," *Renewable and Sustainable Energy Reviews*, vol. 54, pp. 139–150, 2016.

[70] P. Yang and A. Nehorai, "Joint optimization of hybrid energy storage and generation capacity with renewable energy," *IEEE Transactions on Smart Grid*, vol. 5, no. 4, pp. 1566–1574, 2014.

[71] E. Sfikas, Y. Katsigiannis, and P. Georgilakis, "Simultaneous capacity optimization of distributed generation and storage in medium voltage microgrids," *International Journal of Electrical Power & Energy Systems*, vol. 67, pp. 101–113, 2015.

[72] J. Zhu, W. Gu, G. Lou, L. Wang, B. Xu, M. Wu, and W. Sheng, "Learning automata based methodology for optimal allocation of renewable distributed generation considering network reconfiguration," *IEEE Access*, 2017.

[73] C. S. Lai and M. D. McCulloch, "Sizing of stand-alone solar PV and storage system with anaerobic digestion biogas power plants," *IEEE Transactions on Industrial Electronics*, vol. 64, no. 3, pp. 2112–2121, 2017.

[74] A. Askarzadeh, "Electrical power generation by an optimised autonomous PV/wind/tidal/battery system," *IET Renewable Power Generation*, vol. 11, no. 1, pp. 152–164, 2016.

[75] Y. A. Katsigiannis, P. S. Georgilakis, and E. S. Karapidakis, "Hybrid simulated annealing–tabu search method for optimal sizing of autonomous power systems with renewables," *IEEE Transactions on Sustainable Energy*, vol. 3, no. 3, pp. 330–338, 2012.

[76] T. Zhou and W. Sun, "Optimization of battery–supercapacitor hybrid energy storage station in wind/solar generation system," *IEEE transactions on sustainable energy*, vol. 5, no. 2, pp. 408–415, 2014.

[77] A. Abbassi, M. A. Dami, and M. Jemli, "A statistical approach for hybrid energy storage system sizing based on capacity distributions in an autonomous PV/Wind power generation system," *Renewable Energy*, vol. 103, pp. 81–93, 2017.

[78] W. Kellogg, M. Nehrir, G. Venkataramanan, and V. Gerez, "Generation unit sizing and cost analysis for stand-alone wind, photovoltaic, and hybrid wind/PV systems," *IEEE Transactions on energy conversion*, vol. 13, no. 1, pp. 70–75, 1998.

[79] H. Yang, L. Lu, and W. Zhou, "A novel optimization sizing model for hybrid solar-wind power generation system," *Solar energy*, vol. 81, no. 1, pp. 76–84, 2007.

[80] L. Wang and C. Singh, "PSO-based multi-criteria optimum design of a grid-connected hybrid power system with multiple renewable sources of energy," in *Swarm Intelligence Symposium*. IEEE, 2007, pp. 250–257.

[81] J. Kennedy, "Particle swarm optimization," in *Encyclopedia of machine learning*. Springer, 2011, pp. 760–766.

[82] W. Kellogg, M. Nehrir, G. Venkataramanan, and V. Gerez, "Optimal unit sizing for a hybrid wind/photovoltaic generating system," *Electric Power Systems Research*, vol. 39, no. 1, pp. 35–38, 1996.

[83] S. Ahmadi and S. Abdi, "Application of the hybrid big bang–big crunch algorithm for optimal sizing of a stand-alone hybrid pv/wind/battery system," *Solar Energy*, vol. 134, pp. 366–374, 2016.

[84] P. Yang and A. Nehorai, "Joint optimization of hybrid energy storage and generation capacity with renewable energy," *IEEE Transactions on Smart Grid*, vol. 5, no. 4, pp. 1566–1574, 2014.

[85] R. Dufo-López and J. L. Bernal-Agustín, "Multi-objective design of pv–wind–diesel–hydrogen–battery systems," *Renewable energy*, vol. 33, no. 12, pp. 2559–2572, 2008.

[86] H. Yang, W. Zhou, L. Lu, and Z. Fang, "Optimal sizing method for stand-alone hybrid solar–wind system with lpsp technology by using genetic algorithm," *Solar energy*, vol. 82, no. 4, pp. 354–367, 2008.

[87] H. A. Kazem, T. Khatib, and K. Sopian, "Sizing of a standalone photovoltaic/battery system at minimum cost for remote housing electrification in sohar, oman," *Energy and Buildings*, vol. 61, pp. 108–115, 2013.

[88] D. Nelson, M. Nehrir, and C. Wang, "Unit sizing and cost analysis of stand-alone hybrid wind/PV/fuel cell power generation systems," *Renewable energy*, vol. 31, no. 10, pp. 1641–1656, 2006.

[89] O. Ekren and B. Y. Ekren, "Size optimization of a pv/wind hybrid energy conversion system with battery storage using simulated annealing," *Applied Energy*, vol. 87, no. 2, pp. 592–598, 2010.

[90] A. K. Kaviani, G. Riahy, and S. M. Kouhsari, "Optimal design of a reliable hydrogen-based stand-alone wind/PV generating system, considering component outages," *Renewable Energy*, vol. 34, no. 11, pp. 2380–2390, 2009.

[91] A. Maleki and F. Pourfayaz, "Optimal sizing of autonomous hybrid photovoltaic/wind/battery power system with lpsp technology by using evolutionary algorithms," *Solar Energy*, vol. 115, pp. 471–483, 2015.

[92] S. Hakimi and S. Moghaddas-Tafreshi, "Optimal sizing of a stand-alone hybrid power system via particle swarm optimization for kahnouj area in south-east of iran," *Renewable energy*, vol. 34, no. 7, pp. 1855–1862, 2009.

[93] M. Mohammadi, S. Hosseinian, and G. Gharehpetian, "Optimization of hybrid solar energy sources/wind turbine systems integrated to utility grids as microgrid (MG) under pool/bilateral/hybrid electricity market using PSO," *Solar energy*, vol. 86, no. 1, pp. 112–125, 2012.

[94] A. Askarzadeh, "A discrete chaotic harmony search-based simulated annealing algorithm for optimum design of pv/wind hybrid system," *Solar Energy*, vol. 97, pp. 93–101, 2013.

[95] M. Smaoui, A. Abdelkafi, and L. Krichen, "Optimal sizing of stand-alone photovoltaic/wind/hydrogen hybrid system supplying a desalination unit," *Solar Energy*, vol. 120, pp. 263–276, 2015.

[96] A. Fetanat and E. Khorasaninejad, "Size optimization for hybrid photovoltaic–wind energy system using ant colony optimization for continuous domains based integer programming," *Applied Soft Computing*, vol. 31, pp. 196–209, 2015.

[97] S. B. Jeyaprabha and A. I. Selvakumar, "Optimal sizing of photovoltaic/battery/diesel based hybrid system and optimal tilting of solar array using the artificial intelligence for remote houses in india," *Energy and Buildings*, vol. 96, pp. 40–52, 2015.

[98] A. R. Prasad and E. Natarajan, "Optimization of integrated photovoltaic–wind power generation systems with battery storage," *Energy*, vol. 31, no. 12, pp. 1943–1954, 2006.

[99] A. Kaabeche, S. Diaf, and R. Ibtiouen, "Firefly-inspired algorithm for optimal sizing of renewable hybrid system considering reliability criteria," *Solar Energy*, vol. 155, pp. 727–738, 2017.

[100] L. Che, X. Zhang, M. Shahidehpour, A. Alabdulwahab, and Y. Al-Turki, "Optimal planning of loop-based microgrid topology," *IEEE Transactions on Smart Grid*, 2017.

[101] V. Kalkhambkar, R. Kumar, and R. Bhakar, "Joint optimal allocation methodology for renewable distributed generation and energy storage for economic benefits," *IET Renewable Power Generation*, vol. 10, no. 9, pp. 1422–1429, 2016.

[102] F. S. Gazijahani and J. Salehi, "Stochastic multi-objective framework for optimal dynamic planning of interconnected microgrids," *IET Renewable Power Generation*, 2017.

[103] M. R. Aghamohammadi and H. Abdolahinia, "A new approach for optimal sizing of battery energy storage system for primary frequency control of islanded microgrid," *International Journal of Electrical Power & Energy Systems*, vol. 54, pp. 325–333, 2014.

[104] B. Bahmani-Firouzi and R. Azizipanah-Abarghooee, "Optimal sizing of battery energy storage for micro-grid operation management using a new improved bat algorithm," *International Journal of Electrical Power & Energy Systems*, vol. 56, pp. 42–54, 2014.

[105] J. Sachs and O. Sawodny, "Multi-objective three stage design optimization for island microgrids," *Applied Energy*, vol. 165, pp. 789–800, 2016.

[106] R. Dufo-López, J. L. Bernal-Agustín, J. M. Yusta-Loyo, J. A. Domínguez-Navarro, I. J. Ramírez-Rosado, J. Lujano, and I. Aso, "Multi-objective optimiza-

tion minimizing cost and life cycle emissions of stand-alone PV–wind–diesel systems with batteries storage," *Applied Energy*, vol. 88, no. 11, pp. 4033–4041, 2011.

[107] G. Merei, C. Berger, and D. U. Sauer, "Optimization of an off-grid hybrid PV–Wind–Diesel system with different battery technologies using genetic algorithm," *Solar Energy*, vol. 97, pp. 460–473, 2013.

[108] A. Maleki and A. Askarzadeh, "Optimal sizing of a PV/wind/diesel system with battery storage for electrification to an off-grid remote region: A case study of rafsanjan, iran," *Sustainable Energy Technologies and Assessments*, vol. 7, pp. 147–153, 2014.

[109] Y. Katsigiannis, P. Georgilakis, and E. Karapidakis, "Multiobjective genetic algorithm solution to the optimum economic and environmental performance problem of small autonomous hybrid power systems with renewables," *IET Renewable Power Generation*, vol. 4, no. 5, pp. 404–419, 2010.

[110] A. Maheri, "Multi-objective design optimisation of standalone hybrid wind-pv-diesel systems under uncertainties," *Renewable Energy*, vol. 66, pp. 650–661, 2014.

[111] H. Baghaee, M. Mirsalim, G. Gharehpetian, and H. Talebi, "Reliability/cost-based multi-objective Pareto optimal design of stand-alone wind/pv/fc generation microgrid system," *Energy*, vol. 115, pp. 1022–1041, 2016.

[112] H. R. Baghaee, M. Mirsalim, and G. B. Gharehpetian, "Multi-objective optimal power management and sizing of a reliable wind/pv microgrid with hydrogen energy storage using mopso," *Journal of Intelligent & Fuzzy Systems*, vol. 32, no. 3, pp. 1753–1773, 2017.

[113] A. Kaabeche and R. Ibtiouen, "Techno-economic optimization of hybrid photovoltaic/wind/diesel/battery generation in a stand-alone power system," *Solar Energy*, vol. 103, pp. 171–182, 2014.

[114] G. Merei, J. Moshövel, D. Magnor, and D. U. Sauer, "Optimization of self-consumption and techno-economic analysis of pv-battery systems in commercial applications," *Applied Energy*, vol. 168, pp. 171–178, 2016.

[115] T. Mbungu, R. Naidoo, R. Bansal, and M. Bipath, "Optimisation of grid connected hybrid PV-wind-battery system using model predictive control design," *IET Renewable Power Generation*, 2017.

[116] Y.-Y. Hong and R.-C. Lian, "Optimal sizing of hybrid wind/pv/diesel generation in a stand-alone power system using markov-based genetic algorithm," *IEEE Transactions on Power Delivery*, vol. 27, no. 2, pp. 640–647, 2012.

[117] Y. Cao, Y. Zhang, H. Zhang, X. Shi, and V. Terzija, "Probabilistic optimal pv capacity planning for wind farm expansion based on nasa data," *IEEE Transactions on Sustainable Energy*, 2017.

[118] A. Askarzadeh, "Distribution generation by photovoltaic and diesel generator systems: Energy management and size optimization by a new approach for a stand-alone application," *Energy*, vol. 122, pp. 542–551, 2017.

[119] P. Suhane, S. Rangnekar, A. Mittal, and A. Khare, "Sizing and performance analysis of standalone wind-photovoltaic based hybrid energy system using ant colony optimisation," *IET Renewable Power Generation*, vol. 10, no. 7, pp. 964–972, 2016.

[120] M. Mosadeghy, R. Yan, and T. K. Saha, "A time-dependent approach to evaluate capacity value of wind and solar pv generation," *IEEE Transactions on Sustainable Energy*, vol. 7, no. 1, pp. 129–138, 2016.

[121] F. Yang and X. Xia, "Techno-economic and environmental optimization of a household photovoltaic-battery hybrid power system within demand side management," *Renewable Energy*, vol. 108, pp. 132–143, 2017.

[122] S. Kahrobaee, S. Asgarpoor, and W. Qiao, "Optimum sizing of distributed generation and storage capacity in smart households," *IEEE Transactions on Smart Grid*, vol. 4, no. 4, pp. 1791–1801, 2013.

[123] A. Arabali, M. Ghofrani, M. Etezadi-Amoli, and M. S. Fadali, "Stochastic performance assessment and sizing for a hybrid power system of solar/wind/energy storage," *IEEE Transactions on Sustainable Energy*, vol. 5, no. 2, pp. 363–371, 2014.

[124] L. Göransson, S. Karlsson, and F. Johnsson, "Integration of plug-in hybrid electric vehicles in a regional wind-thermal power system," *Energy Policy*, vol. 38, no. 10, pp. 5482–5492, 2010.

[125] Q. Zhang, T. Tezuka, K. N. Ishihara, and B. C. Mclellan, "Integration of PV power into future low-carbon smart electricity systems with EV and HP in Kansai Area, Japan," *Renewable Energy*, vol. 44, pp. 99–108, 2012.

[126] N. Juul and P. Meibom, "Optimal configuration of an integrated power and transport system," *Energy*, vol. 36, no. 5, pp. 3523–3530, 2011.

[127] C. K. Ekman, "On the synergy between large electric vehicle fleet and high wind penetration–an analysis of the Danish case," *Renewable Energy*, vol. 36, no. 2, pp. 546–553, 2011.

[128] R. Atia and N. Yamada, "Sizing and analysis of renewable energy and battery systems in residential microgrids," *IEEE Transactions on Smart Grid*, vol. 7, no. 3, pp. 1204–1213, 2016.

[129] G. Boyle, *Renewable energy*. OXFORD university press, 2004.

[130] A. Arabali, M. Ghofrani, M. Etezadi-Amoli, and M. S. Fadali, "Stochastic performance assessment and sizing for a hybrid power system of solar/wind/energy storage," *IEEE Transactions on Sustainable Energy*, vol. 5, no. 2, pp. 363–371, 2014.

[131] S. Chen, H. B. Gooi, and M. Wang, "Sizing of energy storage for microgrids," *IEEE Transactions on Smart Grid*, vol. 3, no. 1, pp. 142–151, 2012.

[132] S. Shafiq, U. Akram, A. T. Al-Awami, and M. Al-Muhaini, "Reliability evaluation and economic assessment of micro-grid with v2g electric vehicles coordination," in *Smart Grid (SASG), 2016 Saudi Arabia*. IEEE, 2016, pp. 1–7.

[133] B. Zhao, X. Zhang, J. Chen, C. Wang, and L. Guo, "Operation optimization of standalone microgrids considering lifetime characteristics of battery energy storage system," *IEEE Transactions on Sustainable Energy*, vol. 4, no. 4, pp. 934–943, 2013.

[134] S. Rehman, T. Halawani, and T. Husain, "Weibull parameters for wind speed distribution in Saudi Arabia," *Solar Energy*, vol. 53, no. 6, pp. 473–479, 1994.

[135] I. Janajreh, L. Su, and F. Alan, "Wind energy assessment: Masdar city case study," *Renewable energy*, vol. 52, pp. 8–15, 2013.

[136] R. Deng, Z. Yang, J. Chen, N. R. Asr, and M.-Y. Chow, "Residential energy consumption scheduling: A coupled-constraint game approach," *IEEE Transactions on Smart Grid*, vol. 5, no. 3, pp. 1340–1350, 2014.

Vitae

- Name: Umer Akram
- Nationality: Pakistani
- Date of Birth: March, 23^{rd} 1990
- Email: *umer00.akram@gmail.com*
- Permenant Address: Gojra Muzaffarabad Azad Kashmir Pakistan
- Academic Background MS Electrical Engineering, King Fahd University of Petroleum & Minerals Dhahran Saudi Arabia, November 2017

  BS Electrical Engineering COMSATS Institute of Information Technology Abbottabad, Pakistan, 2013